Journal of Human Evolution 133 (2019) 61–77

Contents lists available at ScienceDirect

Journal of Human Evolution

journal homepage: www.elsevier.com/locate/jhevol

Femoral neck and shaft structure in *Homo naledi* from the Dinaledi Chamber (Rising Star System, South Africa)

Lukas Friedl [a], Alex G. Claxton [b], Christopher S. Walker [c, d, e], Steven E. Churchill [e, d], Trenton W. Holliday [f, d], John Hawks [g, d], Lee R. Berger [d], Jeremy M. DeSilva [b, d], Damiano Marchi [h, d, *]

[a] Department of Anthropology, University of West Bohemia, Plzeň, Czech Republic
[b] Department of Anthropology, Dartmouth College, 409 Silsby, HB 6047, Hanover, USA
[c] Department of Molecular Biomedical Sciences, College of Veterinary Medicine, North Carolina State University, 1060 William Moore Drive, Raleigh, NC, 27607, USA
[d] Evolutionary Studies Institute and Centre for Excellence in PalaeoSciences, University of the Witwatersrand, Private Bag 3, Wits, 2050, South Africa
[e] Department of Evolutionary Anthropology, Duke University, 04 Bio Sci Bldg, Durham, NC, 27708, USA
[f] Department of Anthropology, Tulane University, 417 Dinwiddie Hall, New Orleans, LA, 70118, USA
[g] Department of Anthropology, University of Wisconsin, 5325 Sewell Social Science Building, Madison, WI, 53706, USA
[h] Department of Biology, University of Pisa, vis Derna 1, Pisa, 56126, Italy

ARTICLE INFO

Article history:
Received 22 December 2018
Accepted 5 June 2019

Keywords:
Cross-sectional geometry
Lower limb
Bipedal locomotion
Middle Pleistocene

ABSTRACT

The abundant femoral assemblage of *Homo naledi* found in the Dinaledi Chamber provides a unique opportunity to test hypotheses regarding the taxonomy, locomotion, and loading patterns of this species. Here we describe neck and shaft cross-sectional structure of all the femoral fossils recovered in the Dinaledi Chamber and compare them to a broad sample of fossil hominins, recent humans, and extant apes. Cross-sectional geometric (CSG) properties from the femoral neck (base of neck and midneck) and diaphysis (subtrochanteric region and midshaft) were obtained through CT scans for *H. naledi* and through CT scans or from the literature for the comparative sample. The comparison of CSG properties of *H. naledi* and the comparative samples shows that *H. naledi* femoral neck is quite derived with low superoinferior cortical thickness ratio and high relative cortical area. The neck appears superoinferiorly elongated because of two bony pilasters on its superior surface. *Homo naledi* femoral shaft shows a relatively thick cortex compared to the other hominins. The subtrochanteric region of the diaphysis is mediolaterally elongated resembling early hominins while the midshaft is anteroposteriorly elongated, indicating high mobility levels. In term of diaphyseal robusticity, the *H. naledi* femur is more gracile that other hominins and most apes. *Homo naledi* shows a unique combination of characteristics in its femur that undoubtedly indicate a species committed to terrestrial bipedalism but with a unique loading pattern of the femur possibly consequence of the unique postcranial anatomy of the species.

1. Introduction

The discovery of *Homo naledi* in the Dinaledi Chamber of the Rising Star Cave System, South Africa (Berger et al., 2015), provided a rich, though mainly fragmentary, assemblage of fossils with multiple specimens of almost all bones of the postcranial skeleton. The abundance of postcranial material discovered in the Dinaledi Chamber led to a detailed description of the morphology of the species and to some hypotheses about its behavior (Harcourt-Smith et al., 2015; Kivell et al., 2015; Feuerriegel et al., 2017; Marchi et al., 2017; Williams et al., 2017; VanSickle et al., 2018). Primitive shoulder anatomy, low humeral torsion (Feuerriegel et al., 2017), curved phalanges (Kivell et al., 2015), and primitive thoracic (Williams et al., 2017) and pelvic (VanSickle et al., 2018) shape describe a hominin that retained a significant degree of climbing abilities. On the other hand, the long and slender lower limb (Marchi et al., 2017) and the derived foot (Harcourt-Smith et al., 2015) highlight the terrestrial bipedal behavior of *H. naledi*. However, aside from initial descriptions of the Dinaledi Chamber fossil

* Corresponding author.
E-mail address: damiano.marchi@unipi.it (D. Marchi).

https://doi.org/10.1016/j.jhevol.2019.06.002
0047-2484/

material, more detailed biomechanical analyses of the *H. naledi* postcranial skeleton have not yet been provided. The lower limb in particular may answer important questions concerning the locomotor pattern of *H. naledi* and its relationship with other fossil hominins.

The lower limb bones of *H. naledi* show a mix of plesiomorphies (ancestral traits) and apomorphies (derived traits), with few autapomorphies (uniquely derived traits; Harcourt-Smith et al., 2015; Hawks et al., 2017; Marchi et al., 2017; VanSickle et al., 2018). The femur, specifically, is morphologically similar to that of australopiths and early *Homo* in having a relatively long neck, which is also anteroposteriorly compressed and strongly anteverted, but differs in its autapomorphic possession of two bony pillars on the superior neck (Marchi et al., 2017). Characteristics of the femur shared (synapomorphically) with *Homo* species (in particular *Homo erectus*) include well-marked lineae asperae, strong insertion of m. gluteus maximus, and a distal displacement of the minimum diaphyseal breadth of the femur (Marchi et al., 2017). These traits are external morphologies that can be potentially useful in understanding phylogenetic relationships of *H. naledi* with other fossil hominins (Berger et al., 2015; Hawks et al., 2017), though the developmentally plastic nature of limb bones (Losos et al., 2000; Kelly et al., 2006; Langford et al., 2014; Nadell and Shaw, 2016; Pollard et al., 2017, but see Hallgrímsson et al., 2002) makes them less informative than the skull for such purposes.

Primate limb characteristics such as interlimb proportions and linear dimensions, because of their developmental plasticity, have been extensively studied to make inferences about past hominin behavior, in particular locomotion (Stern and Susman, 1983; Jungers, 1985; Latimer et al., 1987; Rose, 1988; Richmond et al., 2002; Haeusler and McHenry, 2004; Harcourt-Smith and Aiello, 2004; Kivell and Schmitt, 2009; Ward et al., 2011). In addition, cross-sectional diaphyseal dimensions have proven to be quite effective in discriminating between locomotor groups in living primates (Ruff, 2002; Marchi, 2010; Marchi et al., 2016) and useful for inferring fossil hominin locomotor behavior (Ruff, 2008, 2009; Marchi et al., 2019).

Long bone cross-sectional properties are highly influenced by actual activity patterns over an individual's lifetime (especially juvenile stages) and change in response to changes in their mechanical loadings (Bertram and Swartz, 1991; Sumner and Andriacchi, 1996; Ruff, 2003; Pearson and Lieberman, 2004; Cowgill et al., 2010; Young et al., 2010; Warden et al., 2014; Sarringhaus et al., 2016). This characteristic makes the structural analysis of limb bone cross-sectional properties well suited for exploring loading patterns, and inferring locomotor patterns and other behaviors, across fossil individuals and species (Trinkaus and Ruff, 1989, 1999; Churchill and Formicola, 1997; Trinkaus and Churchill, 1999; Holt, 2003; Shaw et al., 2012; Ruff et al., 2015, 2016; but see Morimoto et al., 2011). Structural analysis provides insight into the behavior and body shape of past hominin species, which in turn can have taxonomic implications (Ohman et al., 1997; Ruff et al., 1999, 2015; Trinkaus and Ruff, 1999; Trinkaus et al., 1999a, c; Lovejoy et al., 2002; Ruff and Higgins, 2013). One of the major challenges with regard to these efforts, however, is the limited preservation of fossils representing a particular species, individual, or limb element. The discovery of a large number of fossil lower limb bones in the Dinaledi Chamber (Berger et al., 2015) constitutes a unique opportunity to make locomotor, and possibly also taxonomic, inferences about a fossil hominin (*H. naledi*) on the basis of postcranial skeletal elements.

Biomechanical appendicular properties, in particular cross-sectional geometric properties, have been shown to vary with activity (Ruff et al., 1994, 2006; Warden et al., 2005, 2014; Marchi et al., 2006; Sparacello and Marchi, 2008; Shaw and Stock, 2009a, b; Marchi and Shaw, 2011; Sparacello et al., 2018), terrain properties (Ruff, 1999; Marchi, 2008; Sparacello et al., 2008; Holt and Whittey, 2019), age (Ruff and Hayes, 1988; Bouxsein et al., 1994), climatically-induced body proportions (Pearson, 2000a; Stock, 2006), ontogeny (Cowgill et al., 2010; Cowgill, 2014), chronological context (Pearson, 2000a; Trinkaus and Ruff, 2012; Friedl et al., 2016; Marchi et al., 2019), hormones (Wang et al., 2004; Travison et al., 2008), and genetic factors (Pearson, 2000a; Lovejoy et al., 2003). When examining hominin remains, all of these aspects become relevant, and appropriate comparisons should be made based on presumed shared characteristics (i.e., activity, climate, and chronological context). The fossil remains from the Dinaledi Chamber date to the Middle Pleistocene (Dirks et al., 2017), a period in which the African hominin fossil record is extremely sparse (for a review of available evidence see Berger et al., 2017), even more so for postcranial material (and for lower limb bones in particular). The only femora from (likely) Middle Pleistocene Africa preserved enough for such comparisons are the Berg Aukas specimen from Namibia, and two femora from Kabwe in Zambia (Pycraft, 1928; Kennedy, 1984; Grine et al., 1995; Trinkaus et al., 1999b), of which one (Berg Aukas) has been described as somewhat anomalous (Trinkaus et al., 1999b) due to its very low neck-shaft angle and the extremely large femoral head, characteristics matched only by cold-adapted hominins from Middle to Late Pleistocene Europe. Besides these somewhat unusual characteristics, the Berg Aukaus femur aligns well with other Pleistocene femora in having thick diaphyseal cortices and with Late Pleistocene hominins and recent humans in having a short femoral neck (Grine et al., 1995; Trinkaus et al., 1999b). Similar shaft characteristics are present also in the Kabwe femora, which according to Kennedy (1984) align more closely with recent humans than with *H. erectus*.

Femora of earlier members of the genus *Homo* (early *Homo* and to some degree *H. erectus*) are characterized by having thicker cortices compared to modern humans while at the same time being relatively gracile relative to some species from Middle and Late Pleistocene *Homo* (such as *Homo neanderthalensis* and *Homo heidelbergensis*), and by long femoral necks and small heads. Femoral shafts also tend to be mediolaterally elongated in the subtrochanteric region (Ruff, 1995; Trinkaus and Ruff, 2012; Ruff et al., 2015). Earlier hominins (i.e., australopiths) show similar characteristics (Ruff et al., 1999, 2016; Ruff and Higgins, 2013), although there is a substantial amount of variation in all these features among specimens of early *Homo* and among australopiths (Ward et al., 2015). Later Pleistocene hominins present femora that are generally more robust (i.e. showing greater overall diaphyseal strength, see below), are anteroposteriorly reinforced at the midshaft, have shorter and rounder necks with asymmetrical cortical distribution, and have higher neck-shaft angles and larger femoral heads (Trinkaus, 1993; Pearson, 2000b; Holt, 2003; Trinkaus and Ruff, 2012).

The very rich assemblage of *H. naledi* femora from the Dinaledi Chamber (21 adult and eight immature specimens, representing a minimum of eight mature and three immature individuals; Marchi et al., 2017) provides a unique opportunity to characterize the morphology and biomechanical properties of one species of Middle Pleistocene African *Homo*. Recent studies have used femoral neck and diaphyseal cross-sectional properties to make functional and taxonomic inferences about fossil hominins (Trinkaus and Ruff, 2012; Ruff and Higgins, 2013; Ruff et al., 2015). Building upon these previous results, the aims of this paper are: 1) to describe the inner structure of the femoral neck and diaphysis through cross-sectional geometric analysis; 2) to assess the femoral diaphyseal strength and shape of *H. naledi* relative to the other members of the genus *Homo* (and to a lesser degree to australopiths and apes); and 3) to infer the lower limb loading regimes of *H. naledi*.

2. Materials and methods

2.1. The Dinaledi sample

The femoral specimens from the Dinaledi assemblage are curated at the Evolutionary Studies Institute at the University of the Witwatersrand (U.W. in the specimen numbers is after University of the Witwatersrand) and have been described in detail elsewhere (Marchi et al., 2017). Out of the total femoral sample, only adult specimens that preserve key anatomical regions (shaft and/or neck) were included in this study ($n = 9$; Table 1). A subsample was used for the structural analysis of the neck, which included specimens that preserved enough of the proximal diaphysis to identify the longitudinal axis of the diaphysis, as needed to orient the bone following Ruff (2002). These requirements were met in three specimens: U.W. 101-002, U.W. 101-398, and U.W. 101-1391.

Diaphyseal cross-sectional properties were evaluated on specimens that preserved either the subtrochanteric or midshaft regions, or both. Three specimens included the midshaft region (U.W. 101-003, U.W. 101-012, U.W. 101-268) and eight specimens included the subtrochanteric region (U.W. 101-002, U.W. 101-003, U.W. 101-018, U.W. 101-268, U.W. 101-398, U.W. 101-1136, U.W. 101-1391, U.W. 101-1475).

2.2. Comparative samples

The comparative sample consists of a wide array of individual subsamples. The data are derived either from the literature or directly from CT scans in samples that were collected by us, or samples that are publicly available. Comparative samples for the femoral neck include data on South African australopiths and early *Homo* (Ruff and Higgins, 2013, certain neck data that we used and were not reported in tables were derived from their published, scaled images), recent modern humans from the Eneolithic, Bronze Age, and Iron Age of central Europe (EN/IA group; Friedl, 2013), *Gorilla* and *Pongo* from the digital collections of the Smithsonian Institution, and additional metric ape data collected by one of us (A.G.C.). Comparative samples for the diaphysis include recent modern humans (data from Friedl, 2013), fossil hominins (data from Ruff, 2008; Trinkaus and Ruff, 2012; Ruff et al., 2016), and extant ape data (data from Ruff, 2002). More information on comparative samples and individuals is listed in Supplementary Online Material (SOM) Table S1. Some individuals of the comparative EN/IA sample did not have complete neck. Though this did not hamper the collection of diaphyseal cross sections, neck cross sections could not be collected for these specimens. Therefore, analyses on neck properties have been conducted on a subsample of the total EN/IA sample showed in SOM Table S1. Members of the genus *Homo* have been sorted into temporal/specific groups (SOM Table S1): early *Homo*, Middle Paleolithic Modern Humans (MPMH), Neandertals, Early Upper to Middle Upper Paleolithic modern humans (EUP/MUP), and Eneolithic to Iron Age modern humans (EN/IA).

2.3. CT acquisition and processing

Femoral specimens of the Dinaledi sample were CT-scanned using two different setups. CT scans of preserved shafts were scanned at the Department of Radiology, Charlotte Maxeke Hospital, Johannesburg on a Philips Brilliance 64 CT medical scanner (slice thickness 0.9 mm, slice increment 0.45, voltage 120 kV, current 117 μA, reconstructing algorithm facial bone, pixel size 635 μm). Proximal femoral fragments were μCT-scanned on a Nikon Metrology XTH 225/320 LC dual source industrial CT system at the University of the Witwatersrand's Paleosciences Centre (voltage 70 kV, current 120 μA, no filter used, pixel size between 30 and 90 μm). The resolution of CT images might have an effect on the precision of segmentation of the cortical bone from trabecular bone or mineral infill. Therefore, whenever possible we used μCT scans with higher resolution. This proved to be especially important for the femoral neck where cortical bone is thinner than in shafts and there is more trabecular bone that may be confused with cortical bone. As a result, all data on the femoral neck of *H. naledi* came from μCT images. Data on femoral subtrochanteric and midshaft regions are derived from medical CT scans (with the exception of U.W. 101-002 subtrochanteric level, which is also derived from μCT). Although we are aware of the lower resolution of these images, it should not disturb the reliability of the data since, contrary to the structure of the neck, diaphyses contain significantly less trabecular bone (if any) and it has been previously shown (Shaw and Ryan, 2012) that images with low resolution used for cross-sectional analyses produce comparable results to high-resolution images.

Every specimen (i.e., the stack of slices) was oriented into anatomical planes following Ruff (2002) before analysis in order to extract information on anteroposteriorly and mediolaterally oriented variables. Extraction of cross-sectional properties was carried out in Fiji-ImageJ (Schindelin et al., 2012) using the BoneJ plugin (Doube et al., 2010). The automatic segmentation tool available in BoneJ, which works well in sections with a rather low volume of trabecular bone, was used for diaphyses. A combination of automatic and manual segmentation was used for the neck. In a few instances small portions of cortical bone were missing and had to be reconstructed (Fig. 1). In particular, for U.W. 101-1391 very small portions of the cortical bone around the contour of the base of neck

Table 1
Raw cross-sectional diaphyseal properties for the Dinaledi femora.

Specimen	Location	TA	MA	CA	%CA	J	Z_p	I_x	I_y
U.W. 101-002	subtrochanteric	401.0	145.7	255.2	63.7	22,605	1749	9087	13,518
U.W. 101-003	midshaft	351.0	85.8	265.1	75.5	18,582	1571	9181	9401
	subtrochanteric	422.5	96.3	326.2	77.2	29,749	1957	13,008	16,741
U.W. 101-012	midshaft	289.0	39.1	249.9	86.5	13,510	1237	7887	5624
U.W. 101-018	subtrochanteric	327.6	99.5	228.1	69.6	16,114	1342	6270	9844
U.W. 101-268	midshaft	361.4	64.9	296.6	82.1	20,388	1696	11,538	8850
	subtrochanteric	360.5	78.2	282.3	78.3	19,887	1718	8345	11,542
U.W. 101-398	subtrochanteric	389.6	78.2	311.5	79.9	23,673	1919	10,158	13,514
U.W. 101-1136	subtrochanteric	323.1	74.5	248.6	76.9	16,787	1314	6048	10,738
U.W. 101-1391	subtrochanteric	336.0	124.1	211.9	63.1	15,960	1338	6330	9630
U.W. 101-1475	subtrochanteric	416.2	73.3	342.9	82.4	29,420	1948	9099	20,321

Abbreviations: TA = total area; MA = medullary area; CA = cortical area; %CA = percent cortical area (CA/TA *100); J = polar moment of area ($J = I_{max} + I_{min}$); Z_p = polar section modulus; I_x = anteroposterior second moment of area; I_y = mediolateral second moment of area.

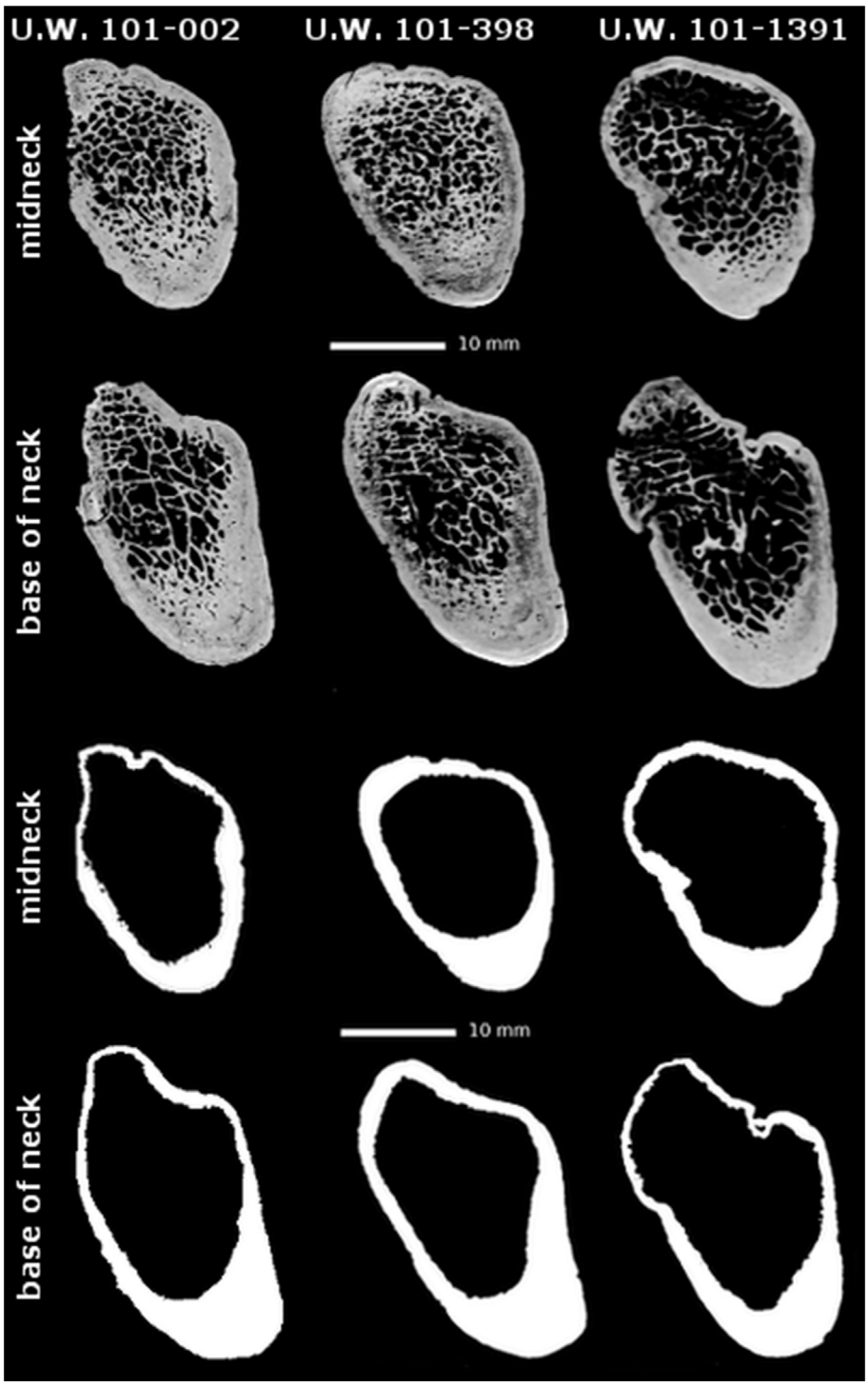

Figure 1. Sample of cross-sectional slices for the Dinaledi femoral neck specimens used in this study (upper two rows) and their binary threshold versions used for generating geometrical properties (lower two rows).

were missing (Fig. 1) and were reconstructed by connecting the periosteal and endosteal contours from both sides of the gap. For U.W. 101-002, the superoanterior cortex was missing at both midneck and base of the neck and it was reconstructed by manually drawing the cortex in Fiji-ImageJ. We followed the general tapering of the cortex observed in the other two *H. naledi* specimens for which the neck was sufficiently preserved (U.W. 101-398 and U.W. 101-1391) to estimate the cortical part missing (see Fig. 1).

2.4. Femur mechanical length estimation and placement of cross-sectional levels in H. naledi *specimens*

Femoral mechanical length is necessary to locate midshaft and subtrochanteric sections, as well as to size-standardize cross-sectional properties (see below). As previously noted (Marchi et al., 2017), all Dinaledi femora are fragmentary. However, using the fragments available it was possible to estimate the mechanical

length of two specimens (U.W. 101-003 and U.W. 101-268). We first created a composite specimen from the U.W. 101-003 and U.W. 102-004—the Lesedi Chamber specimen (Hawks et al., 2017), not included in this study—because they are of very similar size and shape and have overlapping regions (SOM Fig. S1). The composite specimen includes the portion of the diaphysis between the lesser trochanter and the intercondylar fossa. We measured the distance between the most distal part of the lesser trochanter and the most distal margin of the intercondylar fossa (FeLT-IF), in posterior view (SOM Fig. S1) on our sample of complete Eneolithic and Bronze age human femora ($n = 45$) and calculated a regression formula to estimate the femoral mechanical length (FeML) as defined in Ruff (2002) of U.W. 101-003 (RMA regression: FeML = 1.2561 * FeLT-IF − 20.351, $r^2 = 0.96$). The estimated length of U.W. 101-003 using the formula gave a mechanical length of 374.5 mm (95% CI ± 42 mm). The fragmentary U.W. 101-268 specimen is extremely similar in size and shape to the U.W. 101-003 specimen (SOM Fig. S2) so the same length estimate was used for both specimens. U.W. 101-012 preserves less of the proximal shaft than the other two specimens (see Marchi et al., 2017:Fig. 6) and thus we did not feel confident in estimating length in this specimen.

Cross-sectional geometric (CSG) parameters were taken at midshaft (50% of bone mechanical length) and at the subtrochanteric level of the diaphysis (80% of bone mechanical length from distal; Fig. 2), while for the neck we took data at its base and at midneck (Fig. 3). We used two approaches for locating the diaphyseal midshaft and subtrochanteric levels. For U.W. 101-003 we determined midshaft and subtrochanteric levels from the estimated mechanical length. For U.W. 101-268 and for U.W. 101-012, we approximated levels (only midshaft for U.W. 101-012, the subtrochanteric level was too damaged) by side-by-side comparison with the U.W. 101-003 specimen. The proximal fracture of U.W. 101-003 and U.W. 101-268 specimens is just inferior to the lesser trochanter (Marchi et al., 2017); we therefore placed the proximal

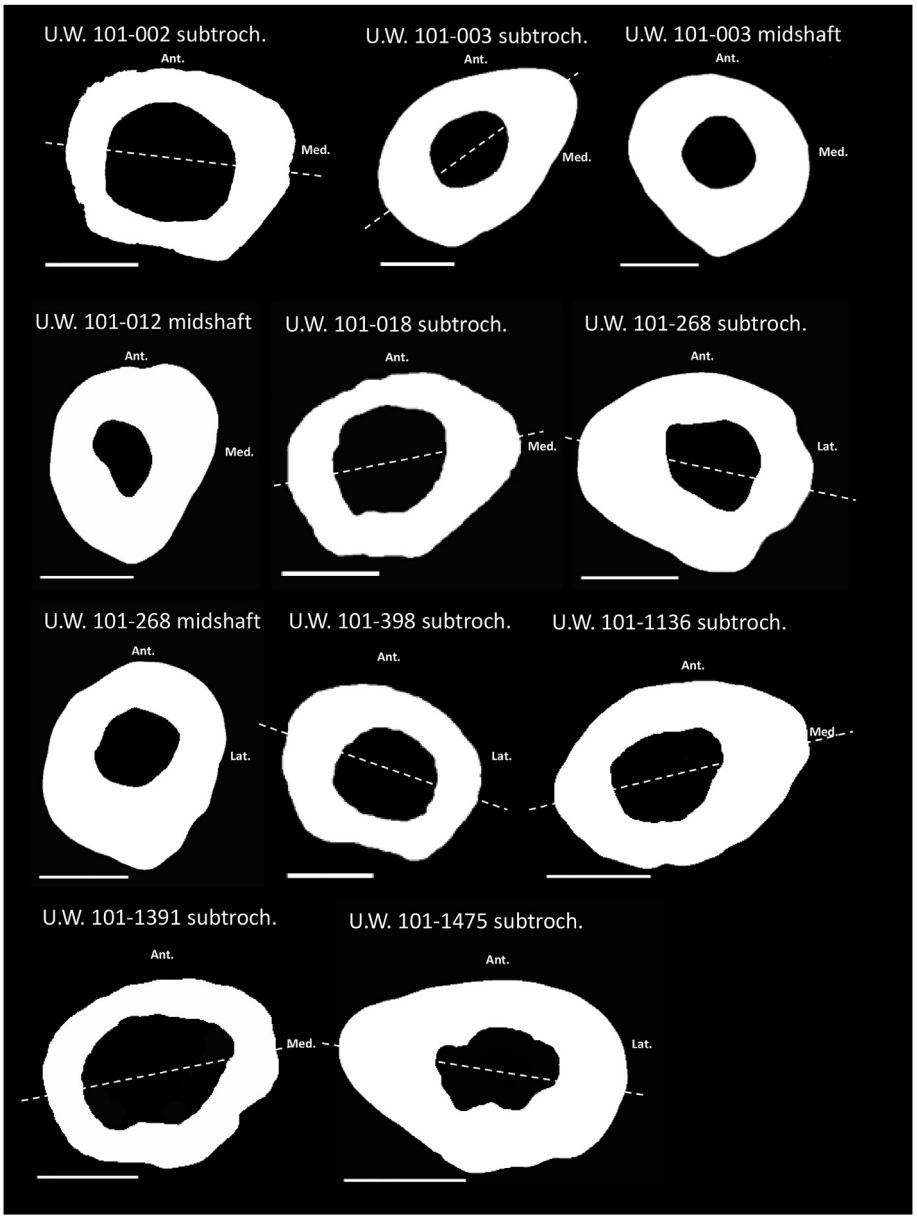

Figure 2. Midshaft and subtrochanteric level cross sections for the eight *Homo naledi* specimens used in this study. Dotted lines show the major axis at the subtrochanteric level.

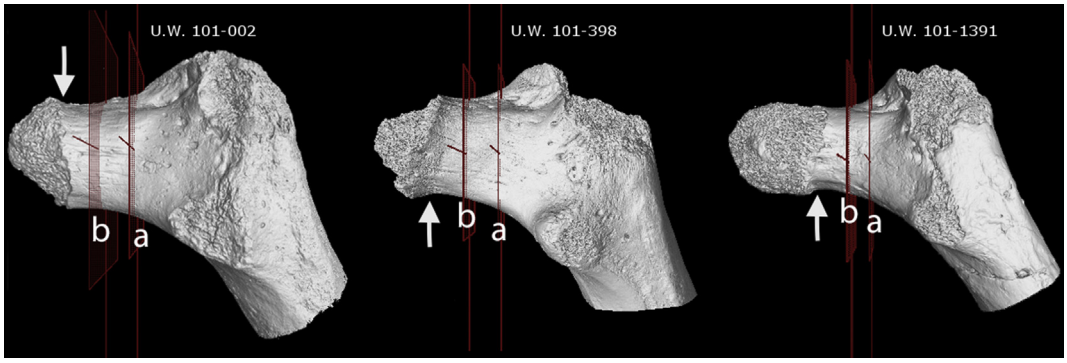

Figure 3. Base of neck (a) and midneck (b) location of the slices for the three Dinaledi proximal femora used in this study. Arrows show the estimated lateral margin of the femoral head.

portion of the two fossils at the same level in the frontal plane and determined the midshaft and subtrochanteric levels of U.W. 101-268 by side-by-side comparison with U.W. 101-003. As for U.W. 101-012, a "break in the bone distally has internal trabeculae indicating proximity to the knee region" (Marchi et al., 2017:179). Indeed we can notice the beginning of the flaring of the diaphysis at the distal break of U.W. 101-012 (Marchi et al., 2017:Fig. 6) and we used such characteristic to position it side-by-side with the combined U.W. 101-003 and U.W. 102-004 femur. We are aware that using this empirical approach to obtain the midshaft level for U.W. 101-268 and for U.W. 101-012 is not as precise as in the case where the entire shaft is available. However, CSG properties do not change dramatically around the central portion of the diaphysis (Sládek et al., 2010); therefore, we feel confident in using such an approximation. Since U.W. 101-012 is not preserved proximally, the subtrochanteric level of the specimen could not be taken.

The second approach was applied to proximal femora that preserve the neck and/or the proximal shaft (U.W. 101-002, U.W. 101-018, U.W. 101-398, U.W. 101-1136, U.W. 101-1391 and U.W. 101-1475). From these, we derived femoral neck levels following a slightly modified procedure described in Ruff and Higgins (2013). Due to the lack of mechanical length estimates for these femora, the subtrochanteric level was approximated as being 10 mm below the lesser trochanter, in the region where there were no more detectable signs of the sloping of the lesser trochanter, following Ruff et al. (1999).

Ruff and Higgins (2013) defined the base of neck as the level just medial to the intertrochanteric line, avoiding the superior flaring of the greater trochanter. The authors defined midneck as the midpoint between the lateral margin of the articular surface of the femoral head and the neck-shaft junction (medial edge of the intertrochanteric line). Since the intertrochanteric line as well as the neck-shaft junction are problematic to see and score on the medical CT images of our comparative samples (EN/IA, gorilla, and orangutan samples), we simplified the procedure by first orienting the CT stack so that the slices run perpendicular to the long axis of the neck, and then designating the slice just before the superior flaring of the greater trochanter as the base of neck. The midneck section was subsequently determined as the midpoint between the base of the neck and lateral margin of the femoral head. In order to be consistent, we used this simplified procedure for our comparative samples as well as for the Dinaledi sample. Figure 3 shows the location of the base and midneck sections on the Dinaledi femora. Since none of the three Dinaledi femora for which we have neck data preserve the femoral head, we estimated the lateral margin of the head. The three specimens preserved at least a small portion of the neck cortex that showed where the head lateral margin was most likely placed (Fig. 3).

2.5. Cross-sectional shape and strength parameters

The diaphyseal CSG properties used in this study were the anteroposterior (AP) second moment of area (I_x) and the mediolateral (ML) second moment of area (I_y), proportional to AP and ML bending rigidity, respectively. Those two variables were used to calculate the diaphyseal shape index (I_x/I_y) of the femur at midshaft. Maximum and minimum second moments of area (I_{max} and I_{min}) were used to calculate the shape index (I_{max}/I_{min}) at the subtrochanteric level. I_{max}/I_{min} is a better shape indicator at the subtrochanteric level than I_x/I_y since the former does not reflect variation in proximal femoral torsion and variation in the neck-shaft angle (Ruff and Hayes, 1983; Holt, 2003; Child, 2017). Cortical distribution in the femoral neck was assessed through relative superior and inferior cortical thickness which is thought to be indicative of the amount and direction of loading placed on the neck (Ruff and Higgins, 2013) and through relative cortical area (%CA = CA/TA × 100, where CA is cortical area and TA is total area of the cross section). %CA was also calculated for the diaphysis. The cross-sectional variable Z_p (section modulus) is used here to evaluate overall femoral strength. These parameters were calculated directly from CT scans for the Dinaledi and Eneolithic to Iron Age samples and taken from published sources for most of the comparative samples (Ruff, 2002, 2008; Trinkaus and Ruff, 2012; Ruff et al., 2016). Since Trinkaus and Ruff (2012) did not report Z_p for the subtrochanteric region in the hominin comparative sample, it is calculated here as polar second moment of area (i.e., $I_x + I_y$) to the power of 0.73 following Ruff (2000a, 2002).

2.6. Size standardization

Mechanical loading of long bones is a function of physical activity, body mass and bone length (Ruff, 2000a). To control the effect of body size, Z_p was scaled by dividing it by the product of body mass and bone mechanical length (Ruff, 2000a). Body mass of the Dinaledi fossils was estimated elsewhere (Garvin et al., 2017) using multivariate estimation methods. Garvin et al. (2017) estimated body mass using two reference samples, one published in Grabowski et al. (2015) based on hominin data and one that was based on Garvin et al.'s (2017) own modern human data. We opted for using Garvin et al.'s (2017) own body mass estimates since those from Grabowski et al. (2015) likely lead to underestimating the true body masses (Ruff et al., 2018). Following Garvin et al (2017: Table 2), the body mass estimates used here are: U.W. 101-003 at 52.9 kg and U.W. 101-268 at 49.3 kg. Body mass of comparative sample individuals was either taken from the literature (Ruff, 2002; Trinkaus and Ruff, 2012) or, for our sample of recent modern humans, estimated following Ruff et al. (2012) using sex-specific

estimation formulae based on the superoinferior femoral head diameter. For individuals with undetermined sex, the combined formula was used.

2.7. Statistical treatment

Due to the small sample size of the fossil material, comparisons between samples were done with the non-parametric Kruskal-Wallis test and the pairwise differences were elucidated through Mann-Whitney U-tests. Although it is common practice to correct for the increased likelihood of making Type I errors in multiple comparisons by adjusting the alpha level (e.g., Bonferroni correction in which the α level is divided by the number of tests performed), we have opted not to do so. Bonferroni corrections are extremely conservative and increase the Type II error rate. Given that we are dealing with small fossil sample sizes (providing little statistical power), and given that non-parametric tests have less power to detect between group differences than do parametric tests, the addition of a conservative Bonferroni adjustment would make it all but impossible to detect significant differences between groups. All the statistical analyses were performed in PAST v. 3.14 (Hammer et al., 2001).

3. Results

3.1. Diaphyseal properties

Table 1 reports raw CSG diaphyseal values for the Dinaledi femora. Figure 4 shows distribution of %CA among hominins for midshaft and subtrochanteric regions. The samples are not significantly different at midshaft (Kruskal-Wallis: $\chi^2 = 7.48$, $p = 0.19$), although *H. naledi* shows on average higher values than the other samples (Fig. 4a). In the subtrochanteric region, *H. naledi* shows among the highest values for %CA but it is significantly greater only compared to the EN/IA sample, which shows significantly lower %CA that the major part of the other samples (Mann-Whitney pairwise comparison; Fig. 4b; Table 2).

Table 3 shows descriptive statistics of femoral midshaft and subtrochanteric shape indices of *H. naledi* compared to the other hominins and apes. *H. naledi* femoral midshaft is anteroposteriorly elongated ($I_x/I_y > 1$) and similar to later Pleistocene hominins such as MPMH and EUP/MUP (Fig. 5a). Great apes and early *Homo* display strongly mediolaterally expanded midshaft cross sections, while Neandertals and EN/IA have a shape close to circularity. There are overall significant differences between samples (Kruskal-Wallis: $\chi^2 = 107.6$, $p < 0.01$): *H. naledi* shows significantly greater values than apes but no significant difference is present when compared with the other hominins (Table 4).

Table 2
Comparison of femoral percent cortical area (%CA = cortical area/total area × 100) at midshaft (above diagonal) and at the subtrochanteric region (below diagonal).[a]

Group	*H. naledi*	Early *Homo*	MPMH	Neandertals	EUP/MUP	EN/IA
H. naledi		0.60	0.38	0.76	0.16	0.07
Early *Homo*	0.54		0.89	0.84	0.85	0.73
MPMH	0.80	0.86		0.79	0.67	0.44
Neandertals	0.73	1.00	0.92		0.11	**0.03**
EUP/MUP	0.66	0.82	0.87	0.96		0.46
EN/IA	**0.04**	0.16	**0.04**	**0.04**	**0.00**	

Abbreviations: MPMH = Middle Paleolithic modern humans; EUP/MUP = Early Upper to Middle Upper Paleolithic modern humans; EN/IA = Eneolithic to Iron Age humans.
[a] Mann-Whitney pairwise comparison, raw *p* values. Significant values bolded.

The femoral subtrochanteric shape of *H. naledi* (no comparison with apes was possible for this location; Table 3) is similar to that of earlier hominins (*Australopithecus afarensis* and *H. erectus*) as well as to Upper Paleolithic and recent modern humans (EUP/MUP and EN/IA samples) in having a relatively large ratio (Table 3; Fig. 5b). An overall significant difference between samples is apparent (Kruskal-Wallis: $\chi^2 = 27.5$, $p < 0.01$) and *H. naledi* displays significantly larger ratio than MPMH and Neanderthals (Table 4).

Table 5 shows midshaft and subtrochanteric descriptive statistics of Z_p standardized by the product of body mass and bone length for *H. naledi* and the comparative samples. The Dinaledi specimens show the smallest mean Z_p values at midshaft compared to the samples analyzed here, with only the early *Homo* sample having a mean (and median) similar to *H. naledi* (though great overlap in individual values is present among groups; Fig. 6a). Significant overall differences were detected between hominin samples (Kruskal-Wallis: $\chi^2 = 15.7$, $p < 0.01$); pairwise comparisons show *H. naledi* to differ from Neandertals (who also differed from some of the other samples; Table 6). When apes are added to the analysis, the overall difference is highly significant ($\chi^2 = 38.2$, $p < 0.01$) with

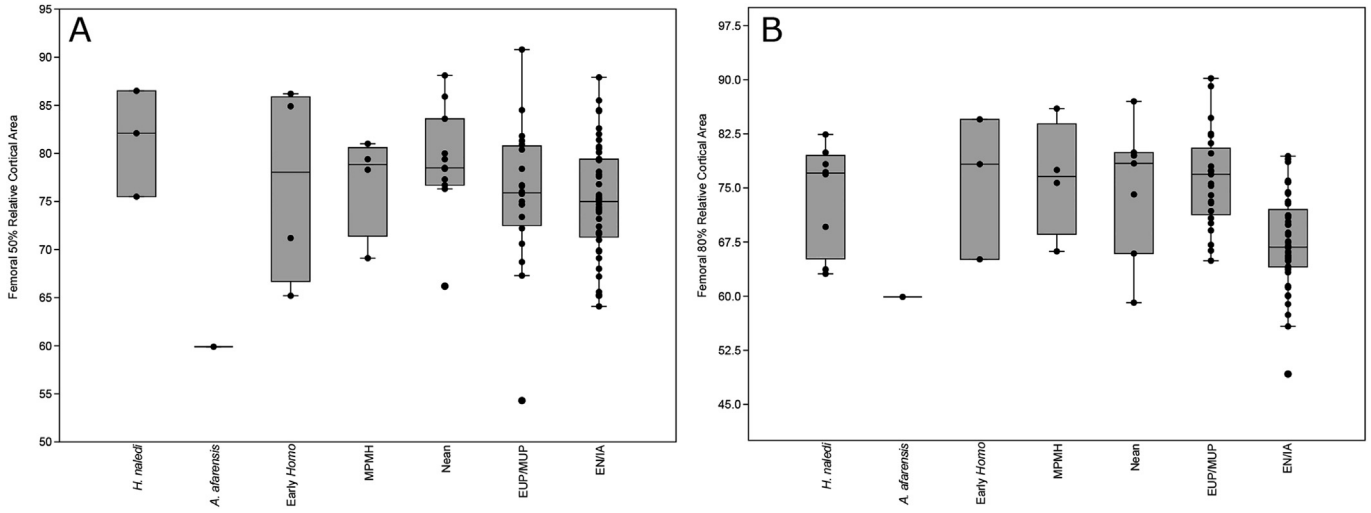

Figure 4. Femoral midshaft (a) and subtrochanteric (b) percent cortical area (%CA = cortical area/total area × 100) distribution among samples. The box-and-whisker plots show the median (dark horizontal line), upper and lower quartile (boxes) and range (whiskers). Black circles represent the value for each specimen.

Table 3
Descriptive statistics for the femoral midshaft and subtrochanteric shape index (I_x/I_y, see text for explanation).

Group	Location	*n*	Mean	SE	SD	Median	CV	Min	Max
H. naledi	midshaft	3	1.23	0.13	0.22	1.30	18.16	0.98	1.40
	subtrochanteric	8	0.65	0.04	0.11	0.66	16.44	0.45	0.78
Early *Homo*	midshaft	4	0.79	0.09	0.17	0.80	21.69	0.59	0.96
	subtrochanteric	3	0.50	0.03	0.05	0.47	10.72	0.46	0.56
MPMH	midshaft	4	1.54	0.11	0.22	1.51	14.06	1.32	1.81
	subtrochanteric	4	0.98	0.09	0.18	1.03	18.70	0.72	1.14
Neandertals	midshaft	11	0.93	0.03	0.12	0.94	12.37	0.70	1.11
	subtrochanteric	7	0.82	0.04	0.10	0.84	11.92	0.67	0.91
EUP/MUP	midshaft	20	1.41	0.07	0.30	1.44	21.10	0.86	1.91
	subtrochanteric	25	0.73	0.03	0.15	0.72	20.33	0.50	1.03
EN/IA	midshaft	45	1.00	0.03	0.20	0.97	19.56	0.66	1.46
	subtrochanteric	45	0.93	0.04	0.26	0.88	27.56	0.48	1.82
Pan	midshaft	23	0.81	0.04	0.21	0.74	26.36	0.51	1.43
Gorilla	midshaft	20	0.58	0.02	0.08	0.58	14.13	0.44	0.72
Pongo	midshaft	20	0.60	0.02	0.09	0.60	14.70	0.46	0.74

Abbreviations: MPMH = Middle Paleolithic modern humans; EUP/MUP = Early Upper to Middle Upper Paleolithic modern humans; EN/IA = Eneolithic to Iron Age humans.

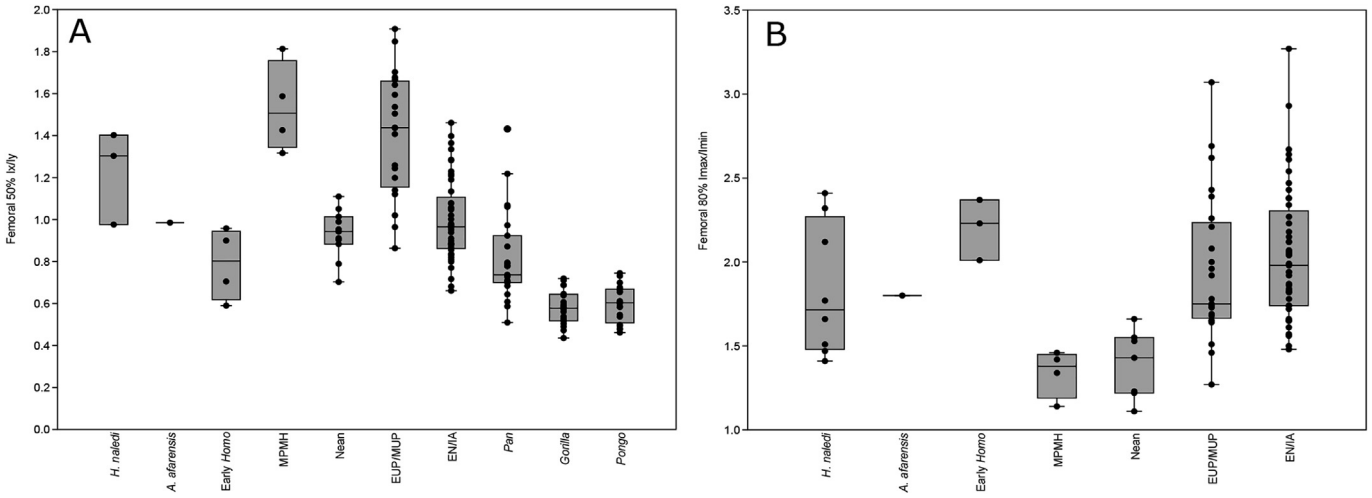

Figure 5. Femoral midshaft (a) Ix/Iy and subtrochanteric (b) Imax/Imin shape indices distribution among hominin and ape samples. The box-and-whisker plots show the median (dark horizontal line), upper and lower quartile (boxes) and range (whiskers). Black circles represent the value for each specimen.

Table 4
Comparisons of femoral shape index (I_x/I_y see text for explanation) at midshaft (above diagonal) and at the subtrochanteric region (below diagonal).[a]

	H. naledi	Early *Homo*	MPMH	Neanderthals	EUP/MUP	EN/IA	*Pan*	*Gorilla*	*Pongo*
H. naledi		0.05	0.11	0.06	0.29	0.07	**0.02**	**0.01**	**0.01**
Early *Homo*	0.08		**0.03**	0.17	**0.00**	0.08	0.92	0.02	0.04
MPMH	**0.03**	0.05		**0.01**	0.56	**0.00**	**0.00**	**0.00**	**0.00**
Neandertals	**0.02**	**0.02**	0.11		**0.00**	0.55	**0.03**	**0.00**	**0.00**
EUP/MUP	0.30	**0.01**	**0.03**	0.08		**0.00**	**0.00**	**0.00**	**0.00**
EN/IA	**0.00**	**0.01**	0.60	0.35	**0.00**		**0.00**	**0.00**	**0.00**
Pan								**0.00**	**0.00**
Gorilla									0.49

Abbreviations: MPMH = Middle Paleolithic modern humans; EUP/MUP = Early Upper to Middle Upper Paleolithic modern humans; EN/IA = Eneolithic to Iron Age humans.
[a] Mann-Whitney pairwise comparison, raw *p* values. Significant values bolded.

pairwise differences variably significant between individual great ape species and hominin samples (Table 6), and *H. naledi* significantly different from *Pan* and *Gorilla*, but not *Pongo*.

At the subtrochanteric region, the Kruskal-Wallis test yielded an overall significant difference ($\chi^2 = 20.2$, $p < 0.01$) between groups. The Dinaledi Chamber specimens again have the smallest mean (and median) values of subtrochanteric robusticity of all the groups (Fig. 6b). In multiple comparisons, *H. naledi* shows significantly smaller subtrochanteric Z_p than the EN/IA group, which together with Neandertals show significant higher values than MPMH and EUP/MUP (Table 7).

3.2. Properties of the neck

Table 7 shows raw cross-sectional data and linear dimensions of the neck for the Dinaledi femora. The comparative samples for the neck analyses differ from those used for the diaphysis. The only sample used for both the diaphysis and neck is the Eneolithic to Iron Age modern humans. Ape data are derived only from the museum specimens for which we were able to get CT scans or direct measurements. Table 8 shows descriptive statistics for the base and midneck %CA. *Homo naledi* shows the highest femoral neck %CA among hominins at both locations, and only *Pongo* shows higher

Table 5
Descriptive statistics for the midshaft and subtrochanteric size-standardized polar section modulus (Z_p).[a]

Group	Location	*n*	Mean	SE	SD	Median	CV	Min	Max
H. naledi	midshaft	2	856	62.8	88.8	856	10.4	793	919
	subtrochanteric	2	959	28.8	40.7	959	4.2	930	988
Early *Homo*	midshaft	4	928	95.9	191.7	912	20.7	734	1154
	subtrochanteric	3	1148	29.9	51.8	1161	4.5	1091	1193
MPMH	midshaft	4	1324	155.9	311.7	1281	23.5	1021	1713
	subtrochanteric	4	1096	62.7	125.3	1092	11.4	954	1244
Neandertals	midshaft	11	1291	70.0	232.0	1343	18.0	991	1655
	subtrochanteric	7	1320	56.8	150.3	1360	11.4	1069	1525
EUP/MUP	midshaft	20	1111	47.1	210.8	1068	19.0	751	1652
	subtrochanteric	20	1126	41.2	184.3	1092	16.4	879	1533
EN/IA	midshaft	45	1063	21.6	144.8	1068	13.6	601	1327
	subtrochanteric	45	1296	27.4	184.0	1308	14.2	764	1667
Pan	midshaft	23	1217	40.2	192.8	1214	15.8	884	1631
Gorilla	midshaft	20	1424	79.0	353.4	1293	24.8	1038	2379
Pongo	midshaft	20	1214	60.2	269.2	1177	22.2	833	1776

Abbreviations: MPMH = Middle Paleolithic modern humans; EUP/MUP = Early Upper to Middle Upper Paleolithic modern humans; EN/IA = Eneolithic to Iron Age humans.
[a] Calculated as [Z_p/(body mass × femoral biomechanical length)] × 10,000.

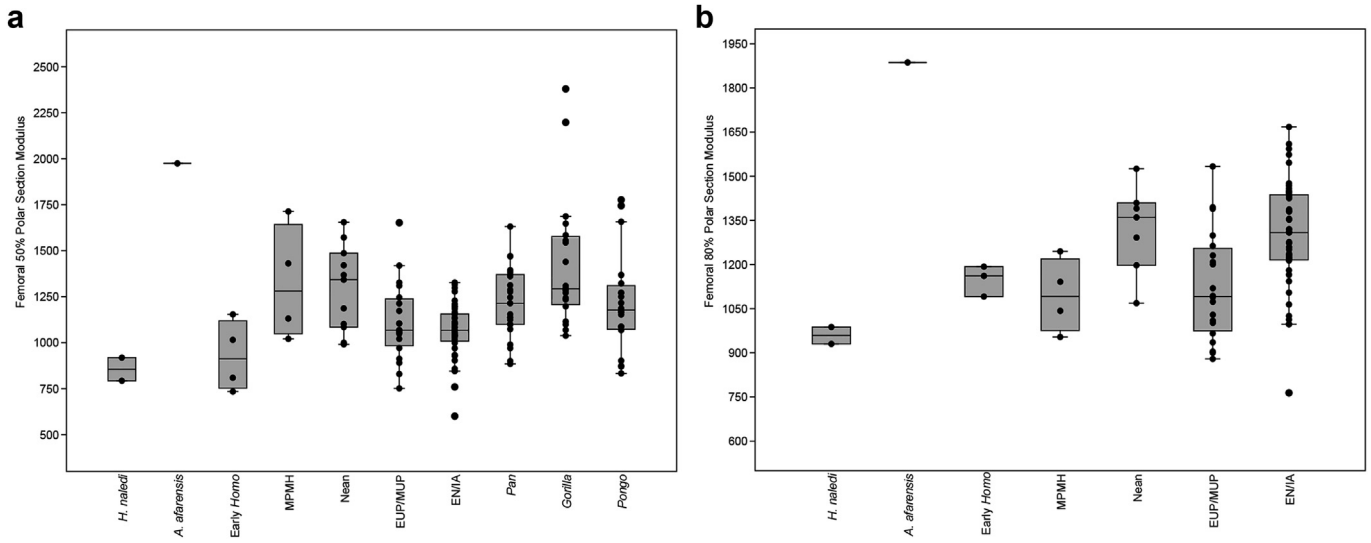

Figure 6. Distribution of femoral midshaft (a) and subtrochanteric (b) polar section modulus (Zp) standardized by a product of body mass (BM) and femur mechanical length (FeBML) for hominin and ape samples. The box-and-whisker plots show the median (dark horizontal line), upper and lower quartile (boxes) and range (whiskers). Black circles represent the value for each specimen.

Table 6
Comparisons of femoral midshaft (above diagonal) and subtrochanteric (below diagonal) size-standardized polar section modulus (Z_p).[a,b]

	H. naledi	Early *Homo*	MPMH	Neanderthals	EUP/MUP	EN/IA	*Pan*	*Gorilla*	*Pongo*
H. naledi		0.82	0.11	**0.04**	0.10	0.05[c]	**0.04**	**0.03**	0.08
Early *Homo*	0.15		0.11	**0.04**	0.11	0.12	**0.03**	**0.01**	**0.03**
MPMH	0.25	0.60		0.74	0.20	0.12	0.56	0.67	0.67
Neandertals	0.06	0.11	**0.05**		**0.05**	**0.01**	0.38	0.42	0.40
EUP/MUP	0.19	0.75	0.97	**0.03**		0.53	0.06	**0.00**	0.16
EN/IA	**0.03**	0.07	**0.03**	0.73	**0.00**		**0.00**	**0.00**	**0.02**
Pan								0.07	0.67
Gorilla									**0.04**

Abbreviations: MPMH = Middle Paleolithic modern humans; EUP/MUP = Early Upper to Middle Upper Paleolithic modern humans; EN/IA = Eneolithic to Iron Age humans.
[a] Calculated as [Z_p/(body mass × femoral biomechanical length)] × 10,000.
[b] Mann-Whitney pairwise comparison, raw *p* values. Significant values bolded.
[c] Nonsignificant difference at $\alpha = 0.05$ before rounding.

values than *H. naledi*. There are overall highly significant differences between samples in %CA at the base as well as at the midneck (Kruskal-Wallis: $\chi^2 = 23.3$, $p < 0.01$ for the base and $\chi^2 = 22.5$, $p < 0.01$ for the midneck). Mann-Whitney pairwise comparisons show for *H. naledi* significantly greater values than for the other hominins at the base of the neck and at midneck, and significantly lower values at the base of the neck and no significant difference at the midneck compared to *Pongo* (Table 9). Figure 7 shows the distribution of %CA among the groups.

Table 10 shows summary statistics of superoinferior cortex ratios of *H. naledi* compared to the other samples at the base of the neck and midneck. In both the base and midneck there are overall

Table 7
Raw neck cross-sectional properties of the Dinaledi femora.[a]

Specimen	Location	TA	MA	CA	%CA	J	Z_p	DSI	DAP	Sup cortex	Inf cortex	S/I ratio
U.W. 101-00	base	356.6	221.1	135.4	38.0	11,649	579	28.1	18.6	0.6	5.3	0.12
	midneck	256.1	172.3	83.8	32.7	5539	369	22.2	15.0	0.8	2.8	0.29
U.W. 101-398	base	328.3	181.6	146.7	44.7	12,785	746	25.6	19.6	1.6	6.5	0.25
	midneck	276.4	166.1	110.3	39.9	8394	642	21.3	17.7	2.3	5.4	0.43
U.W. 101-1391	base	358.6	236.4	122.2	34.1	10,582	554	27.1	20.1	0.6	4.8	0.13
	midneck	302.2	199.9	102.3	33.9	7893	557	23.0	18.7	1.1	3.8	0.29

Abbreviations: TA = total area; MA = medullary area; CA = cortical area; %CA = percent cortical area (CA/TA *100); J = polar moment of area ($J = I_{max} + I_{min}$); Z_p = polar section modulus; DSI = superoinferior diameter of the neck; DAP = anteroposterior diameter of the neck; Sup cortex = thickness of superior cortex; Inf cortex = thickness of inferior cortex; S/I ratio = Sup cortex/Inf cortex.
[a] Linear dimensions in mm (DSI, DAP, Sup cortex and Inf cortex), areas in mm^2, polar moment of area in mm^4, polar section modulus mm^3.

Table 8
Descriptive statistics for the base and midneck percent cortical area (%CA).[a]

Group	Location	*n*	Mean	SE	SD	Median	CV	Min	Max
H. naledi	base of neck	3	38.9	3.1	5.4	38.0	13.8	34.1	44.7
	midneck	3	35.5	2.2	3.9	33.9	10.9	32.7	39.9
Australopithecus[b]	base of neck	5	23.9	2.6	5.8	21.7	24.3	19.6	33.9
	midneck	8	21.8	1.6	4.5	21.9	20.5	16.1	28.4
EN/IA	base of neck	27	28.8	0.7	3.4	29.1	11.8	23.0	34.3
	midneck	27	26.0	0.9	4.8	25.7	18.4	16.2	38.0
Pongo	base of neck	6	69.7	5.0	12.1	70.7	17.4	53.8	87.1
	midneck	6	51.9	5.7	14.1	48.1	27.1	37.9	70.3

Abbreviations: EN/IA = Eneolithic to Iron Age humans.
[a] Calculated as cortical area/total area × 100.
[b] *Australopithecus africanus* and *Australopithecus robustus*.

highly significant differences between samples (Kruskal-Wallis: $\chi^2 = 29.5$, $p < 0.01$ for the base and $\chi^2 = 33.2$, $p < 0.01$ for the midneck). The Dinaledi hominins display the lowest ratio among the comparative hominin and ape samples at the base of the neck (Fig. 8a), meaning *H. naledi* has relatively (to the superior) thicker inferior cortex. They fall below the distribution of South African australopiths and overlap with the lower quartile range of modern humans. Great apes show significantly higher ratios displaying on average equal amounts of cortical bone superiorly and inferiorly (Table 11). A similar pattern is present at midneck, though we observe a larger overlap of *H. naledi* with modern humans (Fig. 8b; Table 11).

For the femoral neck SI to AP breadths analysis, we compared *H. naledi* to the EN/IA, australopiths, *Gorilla*, *Pan*, and *Pongo* samples. We also used data on South African australopiths and early *Homo* from Ruff and Higgins (2013:Table 2), which were not included in the previous analyses. Table 12 shows statistics for the neck SI to AP breadth ratios across samples. *Homo naledi* shows the second highest (after australopiths) ratio (Fig. 9). There are overall significant differences in the SI to AP breadth ratio between samples (Kruskal-Wallis: $\chi^2 = 27.3$, $p < 0.01$). In the pairwise comparisons though, significant differences appear mainly between australopiths and other groups (Table 13).

Table 9
Comparisons of percent cortical area (%CA = cortical area/total area × 100) at the base of neck (above diagonal) and at midneck (below diagonal).[a]

	H. naledi	*Australopithecus*[b]	*H. sapiens*	*Pongo*
H. naledi		**0.04**	**0.01**	**0.03**
Australopithecus[b]	**0.02**		**0.04**	**0.01**
EN/IA	**0.02**	**0.05**		**0.00**
Pongo	0.09	**0.00**	**0.00**	

Abbreviations: EN/IA = Eneolithic to Iron Age humans.
[a] Mann-Whitney pairwise comparison, raw *p* values. Significant values bolded.
[b] *Australopithecus africanus* and *Australopithecus robustus*.

4. Discussion

4.1. Femoral shaft

H. naledi possesses relatively thick cortex at midshaft (high percent cortical area values) similar to Early and Middle Pleistocene hominins and Neandertals. The amount of cortical bone in the femoral shafts of different *Homo* species has been shown to vary only slightly over the course of the Pleistocene. At both midshaft and subtrochanteric levels, there is a slight decrease of thickness at the end of the Pleistocene and into the Holocene (Trinkaus and Ruff, 2012). The reasons why Early and Middle Pleistocene hominins and Neandertals have thicker cortices are still not well understood, primarily due to the complicated processes by which cortical bone is formed during ontogeny and adult. The amount of cortical bone reflects rates of subperiosteal and endosteal apposition and resorption (Ruff and Hayes, 1983, 1988; Feik et al., 2000; Russo et al., 2006; Allen et al., 2012), which themselves are driven by many external and internal factors (e.g., levels of circulating hormones, body mass, activity, health status; Ruff et al., 1994; Moro et al., 1996; van der Meulen et al., 1996; Lieberman, 1997; Pearson and Lieberman, 2004; Devlin et al., 2010; Devlin, 2011; Baab et al., 2018).

Femoral midshaft shape indices (anteroposterior to mediolateral proportions expressed through the ratio of second moments of area, I_x/I_y) are more indicative of functional aspects than percent cortical areas since they reflect the amount of loading through the shaft in a specific direction (Ruff, 2000b). *Homo naledi* shows a midshaft shape index greater than one, meaning their anteroposterior femoral rigidity is higher than mediolateral rigidity. This has been interpreted in the past as a signature of highly mobile populations (Ruff et al., 1984; Sládek et al., 2006a; Sparacello et al., 2011). The Dinaledi hominins are similar to the Middle Paleolithic, Early and Middle Upper Paleolithic and, to a lesser degree, to the Eneolithic to Iron Age modern humans, which are considered (especially the Paleolithic ones) relatively highly mobile groups

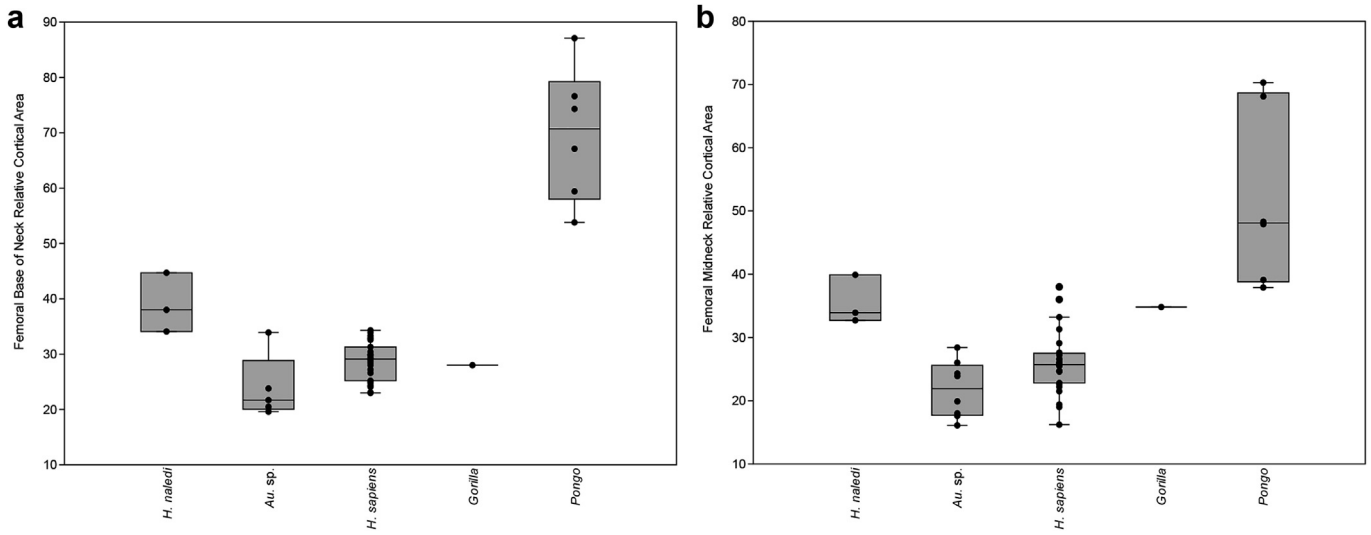

Figure 7. Femoral base of neck (a) and midneck (b) percent cortical area (%CA) distribution among samples. The box-and-whisker plots show the median (dark horizontal line), upper and lower quartile (boxes) and range (whiskers). Black circles represent the value for each specimen.

Table 10
Descriptive statistics for the base and midneck superoinferior cortex ratios.

Group	Location	*n*	Mean	SE	SD	Median	CV	Min	Max
H. naledi	base of neck	3	0.17	0.04	0.07	0.13	43.41	0.12	0.25
	midneck	3	0.34	0.05	0.08	0.29	24.01	0.29	0.43
Australopithecus[a]	base of neck	5	0.40	0.03	0.06	0.42	14.81	0.31	0.47
	midneck	8	0.67	0.07	0.19	0.59	28.75	0.50	1.05
EN/IA	base of neck	27	0.46	0.04	0.21	0.43	46.41	0.18	1.00
	midneck	27	0.47	0.04	0.19	0.45	41.60	0.25	1.33
Pan	base of neck	4	1.03	0.11	0.22	1.04	21.79	0.79	1.24
	midneck	4	0.81	0.13	0.26	0.73	32.74	0.59	1.19
Gorilla	base of neck	4	1.04	0.27	0.53	0.96	51.10	0.48	1.75
	midneck	4	0.93	0.12	0.24	0.89	25.98	0.67	1.25
Pongo	base of neck	6	1.55	0.23	0.56	1.47	36.07	0.95	2.28
	midneck	6	1.01	0.12	0.31	0.94	30.26	0.69	1.43

Abbreviations: EN/IA = Eneolithic to Iron Age humans.
[a] *Australopithecus africanus* and *Australopithecus robustus*.

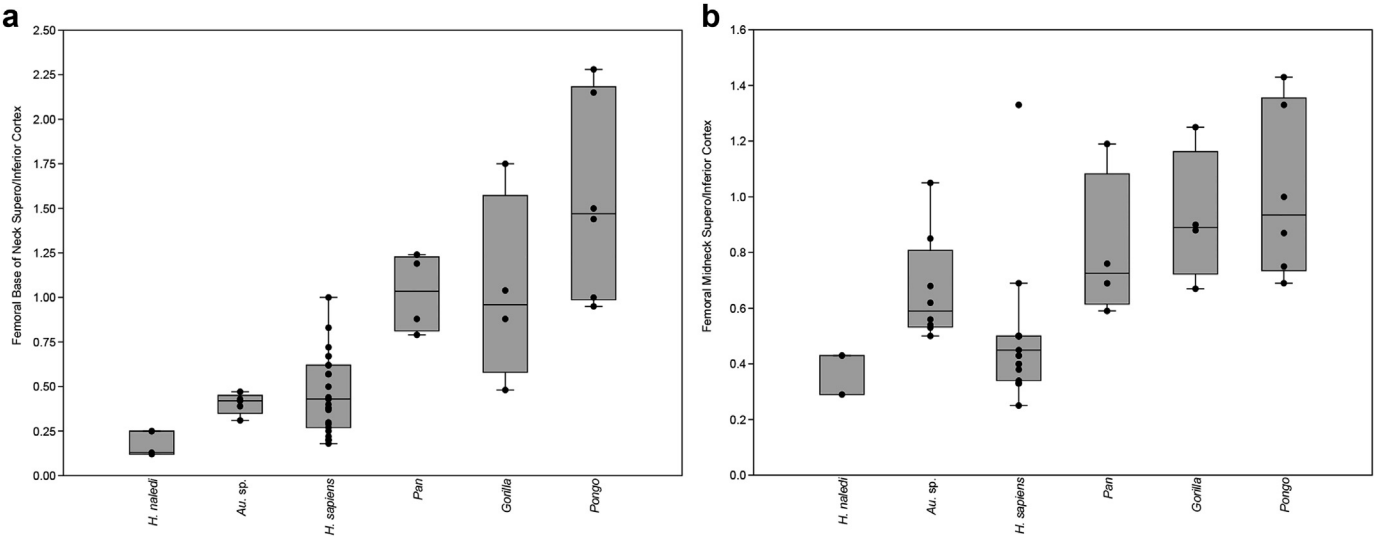

Figure 8. Femoral base of neck (a) and midneck (b) superior/inferior cortex ratio distribution among samples. The box-and-whisker plots show the median (dark horizontal line), upper and lower quartile (boxes) and range (whiskers). Black circles represent the value for each specimen.

Table 11
Comparisons of the superoinferior cortex ratios at the base of the neck (above diagonal) and at midneck (below diagonal).[a]

	H. naledi	*Australopithecus*[c]	*H. sapiens*	*Pan*	*Gorilla*	*Pongo*
H. naledi		**0.04**	**0.02**	0.05[b]	0.05[b]	**0.03**
Australopithecus[c]	**0.02**		0.82	**0.02**	**0.02**	**0.01**
EN/IA	0.06	**0.00**		**0.00**	**0.02**	**0.00**
Pan	**0.05**	0.20	**0.00**		1.00	0.11
Gorilla	**0.05**	0.07	**0.00**	0.47		0.24
Pongo	**0.03**	**0.02**	**0.00**	0.29	0.75	

Abbreviations: EN/IA = Eneolithic to Iron Age humans.
[a] Mann-Whitney pairwise comparison, raw *p* values. Significant values bolded.
[b] Nonsignificant difference at $\alpha = 0.05$ before rounding.
[c] *Australopithecus africanus* and *Australopithecus robustus*.

Table 12
Descriptive statistics for the femoral neck superoinferior to anteroposterior (superoinferior/anteroposterior) breadth ratios.

Group	*n*	Mean	SE	SD	Median	CV	Min	Max
H. naledi	3	1.31	0.09	0.16	1.23	11.90	1.20	1.49
Australopithecus[a]	19	1.35	0.03	0.13	1.34	9.52	1.13	1.63
EN/IA	27	1.13	0.02	0.12	1.12	10.41	0.93	1.36
Gorilla	4	1.21	0.02	0.04	1.22	3.04	1.17	1.25
Pan	4	1.20	0.03	0.07	1.21	5.68	1.12	1.28
Pongo	6	1.24	0.05	0.11	1.24	8.87	1.10	1.38

Abbreviations: EN/IA = Eneolithic to Iron Age humans.
[a] *Australopithecus africanus* and *Australopithecus robustus*.

Table 13
Comparisons for the femoral neck superoinferior to anteroposterior breadth ratios.[a].

	Australopithecus[b]	*H. sapiens*	*Gorilla*	*Pan*	*Pongo*
H. naledi	0.44	0.05	0.60	0.38	0.70
Australopithecus[b]		**0.00**	**0.03**	**0.03**	0.08
EN/IA			0.09	0.21	**0.05**
Gorilla				0.89	0.75
Pan					0.59

Abbreviations: EN/IA = Eneolithic to Iron Age humans.
[a] Mann-Whitney pairwise comparison, raw *p* values. Significant values bolded.
[b] *Australopithecus africanus* and *Australopithecus robustus*.

among modern humans (Holt, 2003; Sládek et al., 2006a, 2006b; Holt and Formicola, 2008; Marchi et al., 2011). The femoral midshaft shape index is also correlated to pelvic breadth (Shaw and Stock, 2011). It has been shown that *H. erectus* and Neandertals have mediolaterally stronger femoral diaphyses due to their increased hip breadth (Ruff, 1995; Weaver, 2003). Wider hips influence primarily the proximal femur through longer moment arms but it is detectable also at midshaft (Ruff, 1995). Shaw and Stock (2011) found that among Late Pleistocene and Holocene hunter-gatherers there is a significant negative correlation between I_x/I_y ratio and pelvic breadth standardized for body mass (as pelvic breadth increases, the I_x/I_y decreases, meaning the shaft becomes stronger in mediolateral relative to anteroposterior direction). Femoral I_x/I_y ratio of *H. naledi* aligns with modern human groups, which have rather narrow pelves optimized for bipedal efficiency. However, discerning whether midshaft shape in *H. naledi* reflects more habitual activities or the influence of pelvic configuration is impossible at present because *H. naledi* pelvic breadth is not yet known. The marked difference between *H. naledi* and any of the ape

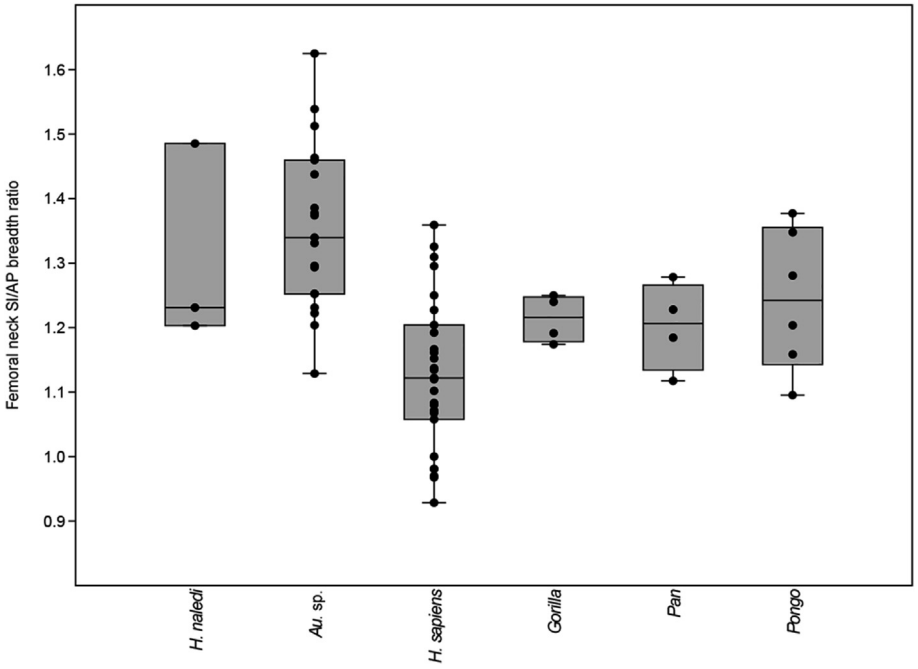

Figure 9. Femoral neck superoinferior (SI) to anteroposterior (AP) neck breadth ratio distribution among samples. The box-and-whisker plots show the median (dark horizontal line), upper and lower quartile (boxes) and range (whiskers). Black circles represent the value for each specimen.

taxa is easier to understand since all of the apes are clearly not as closely related to *H. naledi* as are hominins and have rather different locomotor and postural behaviors (Schultz, 1930; Andrews, 1981), generally causing the forces running through the femoral midshaft to be primarily multilateral to more mediolaterally oriented due to specific position of their femora (e.g., lacking the distal inversion—knees at or closely approaching to the midsagittal plane).

Subtrochanteric I_{max}/I_{min} ratio in *H. naledi* is rather pronounced and resembles that of EUP/MUP, EN/IA, as well as early *Homo* and *A. afarensis* groups. Similarly to what is observed for midshaft I_x/I_y ratio, the Middle Paleolithic groups are significantly different from *H. naledi*, though both groups show substantially rounder subtrochanteric region (at midshaft, the MPMH deviated substantially from circularity as opposed to Neandertals). There is a very good concordance between subtrochanteric I_{max}/I_{min} and I_x/I_y ratios ($r^2 = 0.9$, $p < 0.01$, results not presented here) in *H. naledi* (with the exception of U.W. 101-003, see below). The major axis runs at or very close to the mediolateral axis of the shaft (Fig. 2) indicating mediolateral expansion and anteroposterior compression of the shaft at this level. Such trait is similar to what is found in australopiths (and early *Homo*) and different from later *Homo* and has been explained as the result of larger mediolateral loads in the proximal femur in the formers (Ruff, 1995; Ruff and Higgins, 2013; Ruff et al., 2016). In U.W. 101-003 I_{max}/I_{min} and I_x/I_y are quite dissimilar. The specimen preserves most of its diaphysis but lacks the neck and head. It could have a pronounced head-neck anteversion causing the major axis to be rotated more anteriorly but at present we cannot ascertain its original configuration and therefore the possible reason of the difference of this specimen from the other *H. naledi*. Though a similar subtrochanteric I_{max}/I_{min} ratio is present in early *Homo* (and *H. naledi*) as well as in Upper Paleolithic and Holocene modern humans, the functional significance of this trait is not the same. While for both *H. naledi* and early *Homo*, and for modern humans the major axis of the cross section is oriented mainly mediolaterally, in modern humans (regression between I_{max}/I_{min} and I_x/I_y ratios, $r^2 = 0.00$, $p < 0.92$) we observe a greater variability in the major axis orientation (SOM Fig. S4). This result suggests that the subtrochanteric I_{max}/I_{min} ratio of *H. naledi* reflect functional similarity between its hip region and that of australopiths and early *Homo* (Ruff, 1995; Ruff and Higgins, 2013; Ruff et al., 2016) rather than later modern humans. Given the interrelatedness of the hip traits (femoral neck length, neck-shaft angle, and biacetabular breadth) through effective muscle action during bipedal locomotion (Ruff, 1995), once some of them underwent evolutionary change, the others likely followed soon afterwards to retain integration and functionality of the whole hip region. We suggest that the similarity between *H. naledi* and australopiths (and early *Homo*) in subtrochanteric diaphyseal shape might reflect the fact that the evolutionary transformation of the hip that eventually lead to modern humans had not been initiated (or completed) in the lineage leading to *H. naledi*.

H. naledi has a relatively more gracile femoral diaphysis (as expressed by Z_p), which is most similar to Early Pleistocene early *Homo* and Holocene modern humans. In contrast, Middle to Late Pleistocene groups show a trend toward a relatively more robust femoral diaphysis (Pearson, 2000a, 2000b; Holt, 2003; Trinkaus and Ruff, 2012; Friedl et al., 2016). This increased femoral diaphyseal robusticity was hypothesized to be correlated with a colder climate (Pearson, 2000a; Stock, 2006). Accordingly, the relatively gracile skeleton of *H. naledi* is not surprising in the context of generally warm origins. However, as Ruff and Larsen (2014) note, correlation of robusticity parameters with climate is likely a reflection of variation in body breadth and not a direct relationship between robusticity and climate.

Comparisons with apes reveal that the medium-sized apes (i.e., *Pan* and *Pongo*) overlap with both, smaller and larger-bodied hominins, including *H. naledi*. *Gorilla* appears slightly more robust than *H. naledi* and is similar to some larger-bodied hominins (MPMH and Neandertals). These conclusions may, however, be slightly influenced by the fact that only in hominins the polar section modulus scales isometrically with the product of body mass and bone length. In all the other apes, the scaling follows negative allometry (ordinary least squares regression; SOM Table S2; SOM Fig. S3).

4.2. Femoral neck

While the overall internal morphology of the femoral shaft in *H. naledi* cannot be described as particularly deviating from morphologies seen in other hominin groups, the internal neck morphology showed some substantial differences. The femoral neck of *H. naledi* contains larger quantities of cortical bone than in australopiths and modern humans, and similar amounts to *Gorilla.* The difference in %CA between *H. naledi* and australopiths may in part be caused by the differential methods of reconstruction between the present study, which utilized μCT, and the not-so-well preserved australopith proximal femora presented in Ruff and Higgins (2013), which utilized conventional medical CT and were used here as a source of data. Only *Pongo* has more cortical bone in its neck with *H. naledi* falling in the lower range of its distribution. Further, the ratio between the superior and inferior cortical thickness is the lowest among comparative hominin and ape samples analyzed here, only partially overlapping with modern humans. These two features are directly related because the inferior cortex is very thick causing the overall volume of cortical bone to be large as well as the S/I ratio being very low.

Ruff and Higgins (2013) proposed that the increased SI to AP breadth and relatively thicker superior cortex of the femoral neck is related to increased SI bending forces consequent to more vertically-oriented joint reaction forces. A long femoral neck would also lead to increased SI breadth due to larger bending moments, and the rather low neck-shaft angle (on average 117° in *H. naledi*; Marchi et al., 2017) would contribute to the increase of the neck SI diameter as well. *Homo naledi* shares these latter features with australopiths and some early *Homo* specimens, so one could be tempted to interpret this as evidence of an australopith-like mode of bipedal locomotion where the body's center of gravity is hypothesized to have been tilted laterally a little more than what is typical for *Homo sapiens* (see Ruff and Higgins, 2013).

However, the results of the present study show that the S/I cortex ratio of *H. naledi* significantly deviates from the australopith pattern towards what is typical of *H. sapiens* (which is an obligate terrestrial biped), and possibly indicates human-like (as opposed to more vertical, sensu Ruff and Higgins, 2013) joint reaction forces and an absence of such tilting. There are at least a few factors that complicate our ability to explain the observed pattern in the *H. naledi* femoral neck. First, the cortical distribution in the femoral neck is influenced not only by the forces running through it but also by the distribution and density of trabecular bone inside the neck. The trabecular bone might be more informative of the actual loading patterns than the cortical bone since the former remodels at much higher rate than the latter (Eriksen, 2010) and it may also provide structural stiffness up to 50% of the loads to which the neck is subjected (Lotz et al., 1995). However, several studies of anthropoid primates with different modes of locomotion failed to find a clear correlation between trabecular structure (including in the femoral neck) and predicted loading patterns (Fajardo et al., 2007; Scherf, 2008; Cotter et al., 2009; Ryan and Walker, 2010; DeSilva and Devlin, 2012; Schilling et al., 2013; but see Ryan et al., 2018).

Second, the femoral neck is subject to constraints on multiple levels. As summarized in Kivell (2016), there are lower and upper thresholds for trabecular bone density—to prevent neck fracture and to allow for metabolic and haematopoietic functions (Lotz et al., 1995; Fox and Keaveny, 2001; Currey, 2002) —as well as kinematic limitations on the overall dimensions and cortical thickness of the neck to allow for an optimal functioning of the hip joint (Fox and Keaveny, 2001). Given these limitations, Fox and Keaveny (2001) modeled a functional adaptation of the femoral neck focusing on the eccentric placement of its trabecular bone. The authors hypothesized that the eccentricity resulting in thin superior and thick inferior cortex helps to mitigate risks of fracture by making the inferior aspect of the neck stronger to sustain compressive forces while leaving the superior portion a little more vulnerable to tensile forces, however, not excessively. In their view, such an adaptation might be helpful in maintaining the structural rigidity of the neck even in the face of age-related changes leading to increased risk of fractures.

In summary, the femoral neck in *H. naledi* is rather similar to earlier hominins externally (with the exception of the autapomorphic presence of two pillars on the superior neck) and reminiscent of later *Homo* internally. It is another example of a mosaic nature of morphological evolution throughout the hominin lineage. However, it may be possible that both aspects are functionally related through the presence of the two bony pillars on the superior aspect of the neck of *H. naledi* previously described by Marchi et al. (2017). The slight vulnerability of the superior cortex to tensile forces (sensu Fox and Keaveny, 2001) due to the eccentric placement of trabecular bone inside the neck might in fact be counterbalanced by the presence of the superior bony pillars, especially in a hip joint arrangement similar to that of australopiths for *H. naledi*, as suggested by VanSickle et al. (2018), in which hip joint reaction forces are more vertically oriented and produce higher tensile strains on the superior aspect of the neck (Frankel, 1960; Ruff and Higgins, 2013). Further experimental studies are necessary to test this hypothesis.

Separating phylogenetic signal from functional aspects in morphological characteristics is always a difficult task (Felsenstein, 1985). Especially at low taxonomic levels (ranks) where individual taxa share not only a recent common ancestor but also the propensity for morphological similarities derived from similar genomes (parallelism). Thus, efforts to separate these two aspects are often met with a varying degree of failure (Motani and Schmitz, 2011; Holliday and Friedl, 2013; Ibáñez-Gimeno et al., 2014). One way to minimize the chances of such failure is to abandon efforts to strictly separate phylogenetic and functional aspects of morphology, and rather take them as a unit documenting unique evolutionary trajectory of specific taxa. The case of *H. naledi* is illustrative in this respect. Given what we know about this species, some morphologies have been described as archaic and shared with australopiths (e.g., body mass, brain volume, morphology of the shoulder and thorax, manual phalanges and proximal femur; Kivell et al., 2015; Feuerriegel et al., 2017; Garvin et al., 2017; Marchi et al., 2017; Williams et al., 2017), while other traits are shared with later members of the genus *Homo* (e.g., body size dimorphism, limb proportions, wrist morphology, leg and foot morphology; Harcourt-Smith et al., 2015; Kivell et al., 2015; Garvin et al., 2017; Marchi et al., 2017). Taken together, these unique mosaic combinations of traits not seen in related taxa tell us that *H. naledi*, given its relatively young geological age (236–335 ka; Dirks et al., 2017), must have evolved through a relatively unique evolutionary pathway (Berger et al., 2017). Other recent fossil hominin discoveries from different geographic regions and temporal periods (such as *Homo floresiensis*; Brown et al., 2004) also support the reality that there was greater diversity in the evolution of hominin lineages than previously appreciated.

On the basis of the overall anatomy of the pelvis and lower limb (Harcourt-Smith et al., 2015; Marchi et al., 2017; VanSickle et al., 2018), there is little doubt that *H. naledi* was a proficient bipedal walker. However, the present analysis as well as previous analyses of the femoral and pelvic morphology (Marchi et al., 2017; VanSickle et al., 2018) show that there are characteristics (e.g., lateral iliac flare and external femoral neck morphology) that are not only plesiomorphic but also functionally related to a form of bipedalism practiced by australopiths with a more pronounced lateral tilting of the body's center of gravity (Stern and Susman, 1983; Ruff and Higgins, 2013). This, however, stands in contrast to the evidence from the foot that points to an advanced form of bipedalism, in which body weight is transferred through the hallux preventing the lateral shifting (Harcourt-Smith et al., 2015). It is now understood that non-modern body plans persisted in the hominin lineage until quite late into the Pleistocene (Williams et al., 2017). What is still not resolved is whether these archaic morphologies persisted because they were selectively neutral (hence adaptively insignificant and not transformed into derived states) or because they retained adaptive value and were in fact maintained by stabilizing selection. Contrary to the lower limb, the shoulder and upper limb (arm, forearm and hand) of *H. naledi* preserves a rather archaic morphology (Kivell et al., 2015; Feuerriegel et al., 2017), which has been hypothesized to be retained due to the significant climbing capacity of these hominins. If this was the case, *H. naledi* could have experienced relaxed selection on bipedal efficiency, which would effectively make archaic features of the lower limb selectively neutral or almost neutral. Even then, if we accept that *H. naledi* possessed a form of bipedalism that might have been a bit less effective than that of modern humans (Pontzer et al., 2009) and not fully modern, it probably did not constrain their ability to move around the landscape bipedally.

5. Conclusions

Femoral shaft and neck structure in *H. naledi* provide more detailed evidence about the Middle Pleistocene morphological evolution of lower limb of one lineage of African hominins, for which the fossil record is otherwise very scarce. The internal morphology of the diaphysis shows that *H. naledi* possesses a relatively thicker cortex compared to the other hominin samples analyzed here. The midshaft is anteroposteriorly elongated indicating higher levels of mobility, while the subtrochanteric region is rather mediolaterally elongated, likely as a consequence of specific morphology of the proximal femur and hip region, both producing higher mediolateral bending forces. *Homo naledi* femora are relatively gracile compared to other hominins and apes, although they are not substantially more gracile than other hominins and most apes. The internal morphology of the femoral neck is rather derived in having a very low superoinferior cortical thickness ratio and higher relative cortical area. The superoinferior cortical thickness ratio is similar to recent *H. sapiens* and different from South African australopiths, while the relatively large amount of cortical bone is a trait different from both the hominin groups and shared with apes. The neck is externally superoinferiorly elongated, partially due to the presence of two bony pilasters on its superior aspect. The unique combination of characteristics within the femur is further evidence of mosaic evolution within the hominin lineage and shows that form and function coevolve in a stepwise manner and with different evolutionary pace. Functional interpretations and phylogenetic relatedness are therefore hard to elucidate, especially if not all of the evidence (for example the analysis of trabecular bone in the neck) is taken into account.

Author contributions

D.M. conceived the project. L.F. performed the statistical analysis. L.F., D.M., A.G.C. provided comparative data. All authors participated in the interpretation of results. L.F. and D.M. wrote the paper with contributions from all authors.

Acknowledgements

We thank the National Geographic Society, the Lyda Hill Foundation and the National Research Foundation of South Africa for significantly funding the recovery and study of the remains from Rising Star. The authors wish to thank those who facilitated the collection of the comparative data: B. Zipfel at the Evolutionary Studies Institute, University of the Witwatersrand; P. Velemínský and the Department of Anthropology at the National Museum in Prague, J. Hořejš from the General University Hospital in Prague. This research has been supported by the Grant Agency of the University of West Bohemia (grant number: SGS-2018-033), the Department of Biology, University of Pisa (551-60% 2018).

Supplementary Online Material

Supplementary online material to this article can be found online at https://doi.org/10.1016/j.jhevol.2019.06.002.

References

Allen, M.D., McMillan, S.J., Klein, C.S., Rice, C.L., Marsh, G.D., 2012. Differential age-related changes in bone geometry between the humerus and the femur in healthy men. Aging and Disease 3, 156–163.

Andrews, P.J., 1981. Species diversity and diet in monkeys and apes during the Miocene. In: Stringer, C.B. (Ed.), Aspects of Human Evolution. Taylor & Francis, London, pp. 25–41.

Baab, K.L., Copes, L.E., Ward, D.L., Wells, N., Grine, F.E., 2018. Using modern human cortical bone distribution to test the systemic robusticity hypothesis. Journal of Human Evolution 119, 64–82.

Berger, L.R., Hawks, J., de Ruiter, D.J., Churchill, S.E., Schmid, P., Delezene, L.K., Kivell, T.L., Garvin, H.M., Williams, S.A., DeSilva, J.M., Skinner, M.M., Musiba, C.M., Cameron, N., Holliday, T.W., Harcourt-Smith, W., Ackermann, R.R., Bastir, M., Bogin, B., Bolter, D., Brophy, J., Cofran, Z.D., Congdon, K.A., Deane, A.S., Dembo, M., Drapeau, M., Elliott, M.C., Feuerriegel, E.M., Garcia-Martinez, D., Green, D.J., Gurtov, A., Irish, J.D., Kruger, A., Laird, M.F., Marchi, D., Meyer, M.R., Nalla, S., Negash, E.W., Orr, C.M., Radovcic, D., Schroeder, L., Scott, J.E., Throckmorton, Z., Tocheri, M.W., VanSickle, C., Walker, C.S., Wei, P., Zipfel, B., 2015. *Homo naledi*, a new species of the genus *Homo* from the Dinaledi Chamber, South Africa. eLife 4, e09560.

Berger, L.R., Hawks, J., Dirks, P.H., Elliott, M., Roberts, E.M., 2017. *Homo naledi* and Pleistocene hominin evolution in subequatorial Africa. eLife 6, e24234.

Bertram, J.E.A., Swartz, S.M., 1991. The law of bone transformation: a case of crying Wolff? Biological Reviews 66, 245–273.

Bouxsein, M.L., Myburgh, K.H., van der Meulen, M.C.H., Lindenberger, E., Marcus, R., 1994. Age-related differences in cross-sectional geometry of the forearm bones in healthy Women. Calcified Tissue International 54, 113–118.

Brown, P., Sutikna, T., Morwood, M.J., Soejono, R.P., Jatmiko, Wayhu Saptomo, E., Awe Due, R., 2004. A new small-bodied hominin from the Late Pleistocene of Flores, Indonesia. Nature 431, 1055–1061.

Child, S.L., 2017. Femoral angles and their correlates. PhD Dissertation. University of Missouri.

Churchill, S.E., Formicola, V., 1997. A case of marked bilateral asymmetry in the upper limbs of an Upper Palaeolithic male from Barma Grande (Liguria), Italy. International Journal of Osteoarchaeology 7, 18–38.

Cotter, M.M., Simpson, S.W., Latimer, B.M., Hernandez, C.J., 2009. Trabecular microarchitecture of hominoid thoracic vertebrae. The Anatomical Record 292, 1098–1106.

Cowgill, L.W., 2014. Femoral diaphyseal shape and mobility: an ontogenetic prespective. In: Carslon, J.C., Marchi, D. (Eds.), Reconstructing Mobility: Environmental, Behavioral, and Morphological Determinants. Springer, New York, pp. 193–208.

Cowgill, L.W., Warrener, A., Pontzer, H., Ocobock, C., 2010. Waddling and toddling: The biomechanical effects of an immature gait. American Journal of Physical Anthropology 143, 52–61.

Currey, J.D., 2002. Bones: Structure and Mechanics. Princeton University Press, Princeton.

DeSilva, J.M., Devlin, M.J., 2012. A comparative study of the trabecular bony architecture of the talus in humans, non-human primates, and *Australopithecus*. Journal of Human Evolution 63, 536–551.

Devlin, M.J., 2011. Estrogen, exercise, and the skeleton. Evolutionary Anthropology 20, 54–61.

Devlin, M.J., Stetter, C.M., Lin, H.-M., Beck, T.J., Legro, R.S., Petit, M.A., Lieberman, D.E., Lloyd, T., 2010. Peripubertal estrogen levels and physical activity affect femur geometry in young adult women. Osteoporosis International 21, 609–617.

Dirks, P.H., Roberts, E.M., Hilbert-Wolf, H., Kramers, J.D., Hawks, J., Dosseto, A., Duval, M., Elliott, M., Evans, M., Grün, R., Hellstrom, J., Herries, A.I., Joannes-Boyau, R., Makhubela, T.V., Placzek, C.J., Robbins, J., Spandler, C., Wiersma, J., Woodhead, J., Berger, L.R., 2017. The age of *Homo naledi* and associated sediments in the Rising Star Cave, South Africa. eLife 6, e24231.

Doube, M., Kłosowski, M.M., Arganda-Carreras, I., Cordelières, F.P., Dougherty, R.P., Jackson, J.S., Schmid, B., Hutchinson, J.R., Shefelbine, S.J., 2010. BoneJ: Free and extensible bone image analysis in ImageJ. Bone 47, 1076–1079.

Eriksen, E.F., 2010. Cellular mechanisms of bone remodeling. Reviews in Endocrine and Metabolic Disorders 11, 219–227.

Fajardo, R.J., Müller, R., Ketcham, R.A., Colbert, M., 2007. Nonhuman anthropoid primate femoral neck trabecular architecture and its relationship to locomotor mode. The Anatomical Record 290, 422–436.

Feik, S.A., Thomas, C.D.L., Bruns, R., Clement, J.G., 2000. Regional variations in cortical modeling in the femoral mid-shaft: sex and age differences. American Journal of Physical Anthropology 112, 191–205.

Felsenstein, J., 1985. Phylogenies and the comparative method. The American Naturalist 125, 1–15.

Feuerriegel, E.M., Green, D.J., Walker, C.S., Schmid, P., Hawks, J., Berger, L.R., Churchill, S.E., 2017. The upper limb of *Homo naledi*. Journal of Human Evolution 104, 155–173.

Fox, J.C., Keaveny, T.M., 2001. Trabecular eccentricity and bone adaptation. Journal of Theoretical Biology 212, 211–221.

Frankel, V.H., 1960. The Femoral Neck. Almqvist and Wiksells Boktryckeri AB, Uppsala.

Friedl, L., 2013. The femoral shaft waist, an alternative robusticity measure: its distribution, relation to midshaft, and applicability to behavioral reconstructions. Ph.D. Dissertation, Tulane University.

Friedl, L., Eisová, S., Holliday, T.W., 2016. Re-evaluation of Pleistocene and Holocene long bone robusticity trends with regards to age-at-death estimates and size standardization procedures. Journal of Human Evolution 97, 109–122.

Garvin, H.M., Elliott, M.C., Delezene, L.K., Hawks, J., Churchill, S.E., Berger, L.R., Holliday, T.W., 2017. Body size, brain size, and sexual dimorphism in *Homo naledi* from the Dinaledi Chamber. Journal of Human Evolution 111, 119–138.

Grabowski, M., Hatala, K.G., Jungers, W.L., Richmond, B.G., 2015. Body mass estimates of hominin fossils and the evolution of human body size. Journal of Human Evolution 85, 75–93.

Grine, F.E., Jungers, W.L., Tobias, P.V., Pearson, O.M., 1995. Fossil *Homo* femur from Berg Aukas, northern Namibia. American Journal of Physical Anthropology 97, 151–185.

Haeusler, M., McHenry, H.M., 2004. Body proportions of *Homo habilis* reviewed. Journal of Human Evolution 46, 433–465.

Hallgrímsson, B., Willmore, K., Hall, B.K., 2002. Canalization, developmental stability, and morphological integration in primate limbs. American Journal of Physical Anthropology S 35, 131–158.

Hammer, Ø., Harper, D.A.T., Ryan, P.D., 2001. PAST: Paleontological statistics software package for education and data analysis. Palaeontologia Electronica 4, 4.

Harcourt-Smith, W.E.H., Aiello, L.C., 2004. Fossils, feet and the evolution of human bipedal locomotion. Journal of Anatomy 204, 403–416.

Harcourt-Smith, W.E.H., Throckmorton, Z., Congdon, K.A., Zipfel, B., Deane, A.S., Drapeau, M.S.M., Churchill, S.E., Berger, L.R., DeSilva, J.M., 2015. The foot of *Homo naledi*. Nature Communications 6, 8432.

Hawks, J., Elliott, M., Schmid, P., Churchill, S.E., de Ruiter, D.J., Roberts, E.M., Hilbert-Wolf, H., Garvin, H.M., Williams, S.A., Delezene, L.K., Feuerriegel, E.M., Randolph-Quinney, P., Kivell, T.L., Laird, M.F., Tawane, G., DeSilva, J.M., Bailey, S.E., Brophy, J.K., Meyer, M.R., Skinner, M.M., Tocheri, M.W., VanSickle, C., Walker, C.S., Campbell, T.L., Kuhn, B., Kruger, A., Tucker, S., Gurtov, A., Hlophe, N., Hunter, R., Morris, H., Peixotto, B., Ramalepa, M., van Rooyen, D., Tsikoane, M., Boshoff, P., Dirks, P.H., Berger, L.R., 2017. New fossil remains of *Homo naledi* from the Lesedi Chamber, South Africa. eLife 6, e24232.

Holliday, T.W., Friedl, L., 2013. Hominoid humeral morphology: 3D morphometric analysis. American Journal of Physical Anthropology 152, 506–515.

Holt, B.M., 2003. Mobility in Upper Paleolithic and Mesolithic Europe: evidence from the lower limb. American Journal of Physical Anthropology 122, 200–215.

Holt, B.M., Formicola, V., 2008. Hunters of the Ice Age: The biology of Upper Paleolithic people. American Journal of Physical Anthropology 137, 70–99.

Holt, B.M., Whittey, E., 2019. The impact of terrain on lower limb bone structure. American Journal of Physical Anthropology 168, 729–743.

Ibáñez-Gimeno, P., Galtés, I., Manyosa, J., Malgosa, A., Jordana, X., 2014. Analysis of the forearm rotational efficiency in extant hominoids: New insights into the functional implications of upper limb skeletal structure. Journal of Human Evolution 76, 165–176.

Jungers, W.L., 1985. Body size and scaling of limb proportions in primates. In: Jungers, W.L. (Ed.), Size and Scaling in Primate Biology. Springer, Boston, pp. 345–381.

Kelly, S.A., Czech, P.P., Wight, J.T., Blank, K.M., Garland, T., 2006. Experimental evolution and phenotypic plasticity of hindlimb bones in high-activity house mice. Journal of Morphology 267, 360–374.
Kennedy, G.E., 1984. The emergence of *Homo sapiens* – the post cranial evidence. Man 19, 94–110.
Kivell, T.L., 2016. A review of trabecular bone functional adaptation: what have we learned from trabecular analyses in extant hominoids and what can we apply to fossils? Journal of Anatomy 228, 569–594.
Kivell, T.L., Schmitt, D., 2009. Independent evolution of knuckle-walking in African apes shows that humans did not evolve from a knuckle-walking ancestor. Proceedings of the National Academy of Sciences USA 106, 14241–14246.
Kivell, T.L., Deane, A.S., Tocheri, M.W., Orr, C.M., Schmid, P., Hawks, J., Berger, L.R., Churchill, S.E., 2015. The hand of *Homo naledi*. Nature Communications 6, 8431.
Langford, G.J., Macedonia, J.M., Bessette, C.W., Matey, J.L., Raboin, B.A., Schiffmacher, A.E., Reynolds, B.J., 2014. Phenotypic plasticity in the relative hind-limb growth of lab-reared *Anolis sagrei* : replication of experimental results and a test of perch diameter preference. Journal of Herpetology 48, 228–232.
Latimer, B., Ohman, J.C., Lovejoy, C.O., 1987. Talocrural joint in African hominoids: implications for *Australopithecus afarensis*. American Journal of Physical Anthropology 74, 155–175.
Lieberman, D.E., 1997. Making behavioral and phylogenetic inferences from hominid fossils: considering the developmental influence of mechanical forces. Annual Review of Anthropology 26, 185–210.
Losos, J.B., Creer, D.A., Glossip, D., Goellner, R., Hampton, A., Roberts, G., Haskell, N., Taylor, P., Ettling, J., 2000. Evolutionary implications of phenotypic plasticity in the hindlimb of the lizard *Anolis sagrei*. Evolution 54, 301–305.
Lotz, J.C., Cheal, E.J., Hayes, W.C., 1995. Stress distributions within the proximal femur during gait and falls: implications for osteoporotic fracture. Osteoporosis International 5, 252–261.
Lovejoy, C.O., Meindl, R.S., Ohman, J.C., Heiple, K.G., White, T.D., 2002. The Maka femur and its bearing on the antiquity of human walking: applying contemporary concepts of morphogenesis to the human fossil record. American Journal of Physical Anthropology 119, 97–133.
Lovejoy, C.O., McCollum, M.A., Reno, P.L., Rosenman, B.A., 2003. Developmental biology and human evolution. Annual Review of Anthropology 119, 97–133.
Marchi, D., 2008. Relationships between lower limb cross-sectional geoemetry and mobility: the case of a Neolithic sample from Italy. American Journal of Physical Anthropology 137, 188–200.
Marchi, D., 2010. Articular to diaphyseal proportions of human and great ape metatarsals. American Journal of Physical Anthropology 143, 198–207.
Marchi, D., Shaw, C.N., 2011. Variation in fibular robusticity reflects variation in mobility patterns. Journal of Human Evolution 61, 609–616.
Marchi, D., Sparacello, V., Holt, B.M., Formicola, V., 2006. Biomechanical approach to the reconstruction of activity patterns in Neolithic Western Liguria, Italy. American Journal of Physical Anthropology 131, 447–455.
Marchi, D., Sparacello, V., Shaw, C., 2011. Mobility and lower limb robusticity of a pastoralist Neolithic population from North-Western Italy. In: Pinhasi, R., Stock, J.T. (Eds.), Human Bioarchaeology of the Transition to Agriculture. John Wiley & Sons, Chichester, pp. 317–346.
Marchi, D., Ruff, C.B., Capobianco, A., Rafferty, K.L., Habib, M.B., Patel, B.A., 2016. The locomotion of *Babakotia radofilai* inferred from epiphyseal and diaphyseal morphology of the humerus and femur. Journal of Morphology 277, 1199–1218.
Marchi, D., Walker, C.S., Wei, P., Holliday, T.W., Churchill, S.E., Berger, L.R., DeSilva, J.M., 2017. The thigh and leg of *Homo naledi*. Journal of Human Evolution 104, 174–204.
Marchi, D., Harper, C.M., Chirchir, H., Ruff, C.B., 2019. Relative fibular strength and locomotor behavior in KNM-WT 15000 and OH 35. Journal of Human Evolution 131, 48–60.
Morimoto, N., De León, M.S.P., Zollikofer, C.P.E., 2011. Exploring femoral diaphyseal shape variation in wild and captive chimpanzees by means of morphometric mapping: a test of Wolff's law. The Anatomical Record 294, 589–609.
Moro, M., van der Meulen, M.C.H., Kiratli, B.J., Marcus, R., Bachrach, L.K., Carter, D.R., 1996. Body mass is the primary determinant of midfemoral bone acquisition during adolescent growth. Bone 19, 519–526.
Motani, R., Schmitz, L., 2011. Phylogenetic versus functional signals in the evolution of form-function relationships in terrestrial vision. Evolution 65, 2245–2257.
Nadell, J.A., Shaw, C.N., 2016. Phenotypic plasticity and constraint along the upper and lower limb diaphyses of *Homo sapiens*. American Journal of Physical Anthropology 159, 410–422.
Ohman, J.C., Krochta, T.J., Lovejoy, C.O., Mensforth, R.P., Latimer, B., 1997. Cortical bone distribution in the femoral neck of hominoids: implications for the locomotion of *Australopithecus afarensis*. American Journal of Physical Anthropology 104, 117–131.
Pearson, O.M., 2000a. Activity, climate, and postcranial robusticity: implications for modern human origins and scenarios of adaptative change. Current Anthropology 41, 569–607.
Pearson, O.M., 2000b. Postcranial remains and the origin of modern humans. Evolutionary Anthropology 9, 229–247.
Pearson, O.M., Lieberman, D.E., 2004. The aging of Wolff's "law": ontogeny and responses to mechanical loading in cortical bone. Yearbook of Physical Anthropology 47, 63–99.
Pollard, A.S., Charlton, B.G., Hutchinson, J.R., Gustafsson, T., McGonnell, I.M., Timmons, J.A., Pitsillides, A.A., 2017. Limb proportions show developmental plasticity in response to embryo movement. Scientific Reports 7, 41926.
Pontzer, H., Raichlen, D.A., Sockol, M.D., 2009. The metabolic cost of walking in humans, chimpanzees, and early hominins. Journal of Human Evolution 56, 43–54.
Pycraft, W.P., 1928. Rhodesian Man: Description of the skull and other human remains from Broken Hill. In: Pycraft, W.P., Elliot Smith, G., Yearsley, M., Carter, J.T., Smith, R.A., Hopwood, A.T., Bate, D.M.A., Swinton, W.E. (Eds.), Rhodesian Man and Associated Remains. British Museum, London, pp. 1–51.
Richmond, B.G., Aiello, L.C., Wood, B.A., 2002. Early hominin limb proportions. Journal of Human Evolution 43, 529–548.
Rose, M.D., 1988. Functional anatomy of the cheiridia. In: Schwartz, J.H. (Ed.), Orangutan Biology. Oxford University Press, New York, pp. 299–310.
Ruff, C.B., 1995. Biomechanics of the hip and birth in early *Homo*. American Journal of Physical Anthropology 98, 527–574.
Ruff, C.B., 1999. Skeletal structure and behavioral patterns of prehistoric Great Basin populations. In: Hemphill, B.E., Larsen, C.S. (Eds.), Understanding Prehistoric Lifeways in the Great Basin Wetlands: Bioarchaeological Reconstruction and Interpretation. University Utah Press, Salt Lake City, pp. 290–320.
Ruff, C.B., 2000a. Body size, body shape, and long bone strength in modern humans. Journal of Human Evolution 38, 269–290.
Ruff, C.B., 2000b. Biomechanical analyses of archaeological human skeletons. In: Katzenberg, M.A., Saunders, S.R. (Eds.), Biological Anthropology of the Human Skeleton. John Wiley & Sons, New York, pp. 71–102.
Ruff, C.B., 2002. Long bone articular and diaphyseal structure in Old World monkeys and apes. I: locomotor effects. American Journal of Physical Anthropology 119, 305–342.
Ruff, C.B., 2003. Ontogenetic adaptation to bipedalism: age changes in femoral to humeral length and stregth proportions in humans, with a comparison to baboons. Journal of Human Evolution 45, 317–349.
Ruff, C.B., 2008. Femoral/humeral strength in early African *Homo erectus*. Journal of Human Evolution 54, 383–390.
Ruff, C.B., 2009. Relative limb strength and locomotion in *Homo habilis*. American Journal of Physical Anthropology 138, 90–100.
Ruff, C.B., Hayes, W.C., 1983. Cross-sectional geometry of Pecos Pueblo femora and tibiae – a biomechanical investigation: II. sex, age, and side differences. American Journal of Physical Anthropology 60, 383–400.
Ruff, C.B., Hayes, W.C., 1988. Sex differences in age-related remodeling of the femur and tibia. Journal of Orthopaedic Research: Official Publication of the Orthopaedic Research Society 6, 886–896.
Ruff, C.B., Higgins, R., 2013. Femoral neck structure and function in early hominins. American Journal of Physical Anthropology 150, 512–525.
Ruff, C.B., Larsen, C.S., 2014. Long bone structural analyses and the reconstruction of past mobility: A historical review. In: Carlson, K.J., Marchi, D. (Eds.), Reconstructing Mobility: Environmental, Behavioral, and Morphological Determinants. Springer US, New York, pp. 13–29.
Ruff, C.B., Larsen, C.S., Hayes, W.C., 1984. Structural changes in the femur with the transition to agriculture on the Georgia coast. American Journal of Physical Anthropology 64, 125–136.
Ruff, C.B., Walker, A., Trinkaus, E., 1994. Postcranial robusticity in *Homo*, III: Ontogeny. American Journal of Physical Anthropology 93, 35–54.
Ruff, C.B., McHenry, H.M., Thackeray, J.F., 1999. Cross-sectional morphology of the SK 82 and 97 proximal femora. American Journal of Physical Anthropology 109, 509–521.
Ruff, C.B., Holt, B.M., Trinkaus, E., 2006. Who's afraid of the big bad wolff?: "Wolff's Law" and bone functional adaptation. American Journal of Physical Anthropology 129, 484–498.
Ruff, C.B., Holt, B.M., Niskanen, M., Sladek, V., Berner, M., Garofalo, E., Garvin, H.M., Hora, M., Maijanen, H., Niinimaki, S., Salo, K., Schuplerova, E., Tompkins, D., 2012. Stature and body mass estimation from skeletal remains in the European Holocene. American Journal of Physical Anthropology 148, 601–617.
Ruff, C.B., Puymerail, L., Macchiarelli, R., Sipla, J., Ciochon, R.L., 2015. Structure and composition of the Trinil femora: functional and taxonomic implications. Journal of Human Evolution 80, 147–158.
Ruff, C.B., Burgess, M.L., Ketcham, R.A., Kappelman, J., 2016. Limb bone structural proportions and locomotor behavior in A.L. 288-1 ("Lucy"). PLoS ONE 11, e0166095.
Ruff, C.B., Burgess, M.L., Squyres, N., Junno, J.-A., Trinkaus, E., 2018. Lower limb articular scaling and body mass estimation in Pliocene and Pleistocene hominins. Journal of Human Evolution 115, 85–111.
Russo, C.R., Lauretani, F., Seeman, E., Bartali, B., Bandinelli, S., Di Iorio, A., Guralnik, J., Ferrucci, L., 2006. Structural adaptations to bone loss in aging men and women. Bone 38, 112–118.
Ryan, T.M., Walker, A., 2010. Trabecular bone structure in the humeral and femoral heads of anthropoid primates. The Anatomical Record 293, 719–729.
Ryan, T.M., Carlson, K.J., Gordon, A.D., Jablonski, N., Shaw, C.N., Stock, J.T., 2018. Human-like hip joint loading in *Australopithecus africanus* and *Paranthropus robustus*. Journal of Human Evolution 121, 12–24.
Sarringhaus, L.A., MacLatchy, L.M., Mitani, J.C., 2016. Long bone cross-sectional properties reflect changes in locomotor behavior in developing chimpanzees. American Journal of Physical Anthropology 160, 16–29.
Scherf, H., 2008. Locomotion-related femoral trabecular architectures in primates — high resolution computed tomographies and their implications for estimations

of locomotor preferences of fossil primates. In: Endo, H., Frey, R. (Eds.), Anatomical Imaging. Springer, Tokio, pp. 39–59.
Schilling, A.-M., Tofanelli, S., Hublin, J.-J., Kivell, T.L., 2013. Trabecular bone structure in the primate wrist. Journal of Morphology 275, 572–585.
Schindelin, J., Arganda-Carreras, I., Frise, E., Kaynig, V., Longair, M., Pietzsch, T., Preibisch, S., Rueden, C., Saalfeld, S., Schmid, B., Tinevez, J.-Y., White, D.J., Hartenstein, V., Eliceiri, K., Tomancak, P., Cardona, A., 2012. Fiji: an open-source platform for biological-image analysis. Nature Methods 9, 676–682.
Schultz, A.H., 1930. The skeleton of the trunk and limbs of higher primates. Human Biology 2, 303–438.
Shaw, C.N., Ryan, T.M., 2012. Does skeletal anatomy reflect adaptation to locomotor patterns? Cortical and trabecular architecture in human and nonhuman anthropoids. American Journal of Physical Anthropology 147, 187–200.
Shaw, C.N., Stock, J.T., 2009a. Intensity, repetitiveness, and directionality of habitual adolescent mobility patterns influence the tibial diaphysis morphology of athletes. American Journal of Physical Anthropology 140, 149–159.
Shaw, C.N., Stock, J.T., 2009b. Habitual throwing and swimming correspond with upper limb diaphyseal strength and shape in modern human athletes. American Journal of Physical Anthropology 140, 160–172.
Shaw, C.N., Stock, J.T., 2011. The influence of body proportions on femoral and tibial midshaft shape in hunter-gatherers. American Journal of Physical Anthropology 144, 22–29.
Shaw, C.N., Hofmann, C.L., Petraglia, M.D., Stock, J.T., Gottschall, J.S., 2012. Neandertal humeri may reflect adaptation to scraping tasks, but not ppear thrusting. PLoS One 7, e40349.
Sládek, V., Berner, M., Sailer, R., 2006a. Mobility in central European Late Eneolithic and Early Bronze Age: Femoral cross-sectional geometry. American Journal of Physical Anthropology 130, 320–332.
Sládek, V., Berner, M., Sailer, R., 2006b. Mobility in Central European Late Eneolithic and Early Bronze Age: Tibial cross-sectional geometry. Journal of Archaeological Science 33, 470–482.
Sládek, V., Berner, M., Galeta, P., Friedl, L., Kudrnová, Š., 2010. Technical note: The effect of midshaft location on the error ranges of femoral and tibial cross-sectional parameters. American Journal of Physical Anthropology 141, 325–332.
Sparacello, V., Marchi, D., 2008. Mobility and subsistence economy: A diachronic comparison between two groups settled in the same geographical area (Liguria, Italy). American Journal of Physical Anthropology 136, 485–495.
Sparacello, V.S., Pearson, O.M., Petersen, T.R., 2008. Untangling the effects of terrain and mobility on the cross-sectional geometry of femur and tibia. American Journal of Physical Anthropology S46, 199.
Sparacello, V.S., Pearson, O.M., Coppa, A., Marchi, D., 2011. Changes in skeletal robusticity in an iron age agropastoral group: The samnites from the Alfedena necropolis (Abruzzo, Central Italy). American Journal of Physical Anthropology 144, 119–130.
Sparacello, V., Villotte, S., Shaw, C., Federica, F., Mottes, E., Starnini, E., Giampaolo, D., Marchi, D., 2018. Changing mobility patterns at the Pleistocene-Holocene transition. In: Borgia, V., Cristiani, E. (Eds.), Paleolithic Italy. Advanced Studies on Early Human Adaptations in the Apennine Peninsula. Sidestone Press, Leiden, pp. 357–396.
Stern Jr., J.T., Susman, R.L., 1983. The locomotor anatomy of *Australopithecus afarensis*. American Journal of Physical Anthropology 60, 279–317.
Stock, J.T., 2006. Hunter-gatherer postcranial robusticity relative to patterns of mobility, climatic adaptation, and selection for tissue economy. American Journal of Physical Anthropology 131, 194–204.
Sumner, D.R., Andriacchi, T.P., 1996. Adaptation to defferential loading: comparison of growth-related changes in cross-sectional properties of the human femur and humerus. Bone 19, 121–126.
Travison, T.G., Araujo, A.B., Beck, T.J., Williams, R.E., Clark, R.V., Leder, B.Z., McKinlay, J.B., 2008. Relation between serum testosterone, serum estradiol, sex hormone-binding globulin, and geometrical measures of adult male proximal femur strength. The Journal of Clinical Endocrinology & Metabolism 94, 853–860.
Trinkaus, E., 1993. Femoral neck-shaft angles of the Qafzeh-Skhul early modern humans, and activity levels among immature Near Eastern Middle Paleolithic hominids. Journal of Human Evolution 25, 393–416.
Trinkaus, E., Churchill, S.E., 1999. Diaphyseal cross-sectional geometry of Near Eastern middle Palaeolithic humans: The humerus. Journal of Archaeological Science 26, 173–184.
Trinkaus, E., Ruff, C.B., 1989. Diaphyseal cross-sectional morphology and biomechanics of the Fond-de-Foret 1 femur and the Spy 2 femur and tibia. Bulletin de la Société Royale d'Anthopologie et de Préhistoire 100, 33–42.
Trinkaus, E., Ruff, C.B., 1999. Diaphyseal cross-sectional geometry of Near Eastern middle Palaeolithic humans: The femur. Journal of Archaeological Science 26, 409–424.
Trinkaus, E., Ruff, C.B., 2012. Femoral and tibial diaphyseal cross-sectional geometry in Pleistocene *Homo*. PaleoAnthropology 2012, 13–62.
Trinkaus, E., Churchill, S.E., Ruff, C.B., Vandermeersch, B., 1999a. Long bone shaft robusticity and body proportions of the Saint-Césaire 1 Chatelperronian Neanderthal. Journal of Archaeological Science 26, 753–773.
Trinkaus, E., Ruff, C.B., Conroy, G.C., 1999b. The anomalous archaic *Homo* femur from Berg Aukas, Namibia: a biomechanical assessment. American Journal of Physical Anthropology 110, 379–391.
Trinkaus, E., Stringer, C.B., Ruff, C.B., Hennessy, R.J., Roberts, M.B., Parfitt, S.A., 1999c. Diaphyseal cross-sectional geometry of the Boxgrove 1 Middle Pleistocene human tibia. Journal of Human Evolution 37, 1–25.
van der Meulen, M.C.H., Ashford, M.W., Kiratli, B.J., Bachrach, L.K., Carter, D.R., 1996. Determinants of femoral geometry and structure during adolescent growth. Journal of Orthopaedic Research 14, 22–29.
VanSickle, C., Cofran, Z., García-Martínez, D., Williams, S.A., Churchill, S.E., Berger, L.R., Hawks, J., 2018. *Homo naledi* pelvic remains from the Dinaledi Chamber, South Africa. Journal of Human Evolution 125, 122–136.
Wang, Q., Nicholson, P.H.F., Suuriniemi, M., Lyytikäinen, A., Helkala, E., Alen, M., Suominen, H., Cheng, S., 2004. Relationship of sex hormones to bone geometric properties and mineral density in early pubertal girls. The Journal of Clinical Endocrinology & Metabolism 89, 1698–1703.
Ward, C.V., Kimbel, W.H., Johanson, D.C., 2011. Complete fourth metatarsal and arches in the foot of *Australopithecus afarensis*. Science 331, 750–753.
Ward, C.V., Feibel, C.S., Hammond, A.S., Leakey, L.N., Moffett, E.A., Plavcan, J.M., Skinner, M.M., Spoor, F., Leakey, M.G., 2015. Associated ilium and femur from Koobi Fora, Kenya, and postcranial diversity in early *Homo*. Journal of Human Evolution 81, 48–67.
Warden, S.J., Hurst, J.A., Sanders, M.S., Turner, C.H., Burr, D.B., Li, J., 2005. Bone adaptation to a mechanical loading program significantly increases skeletal fatigue resistance. Journal of Bone and Mineral Research 20, 809–816.
Warden, S.J., Mantila Roosa, S.M., Kersh, M.E., Hurd, A.L., Fleisig, G.S., Pandy, M.G., Fuchs, R.K., 2014. Physical activity when young provides lifelong benefits to cortical bone size and strength in men. Proceedings of the National Academy of Sciences USA 111, 5337–5342.
Weaver, T.D., 2003. The shape of the Neandertal femur is primarily the consequence of a hyperpolar body form. Proceedings of the National Academy of Sciences USA 100, 6926–6929.
Williams, S.A., García-Martínez, D., Bastir, M., Meyer, M.R., Nalla, S., Hawks, J., Schmid, P., Churchill, S.E., Berger, L.R., 2017. The vertebrae and ribs of *Homo naledi*. Journal of Human Evolution 104, 136–154.
Young, J.W., Fernández, D., Fleagle, J.G., 2010. Ontogeny of long bone geometry in capuchin monkeys (*Cebus albifrons* and *Cebus apella*): implications for locomotor development and life history. Biology Letters 6, 197–200.